Article

Structure

Deep Structural Analysis of RPAP3 and PIH1D1, Two Components of the HSP90 Co-chaperone R2TP Complex

Graphical Abstract

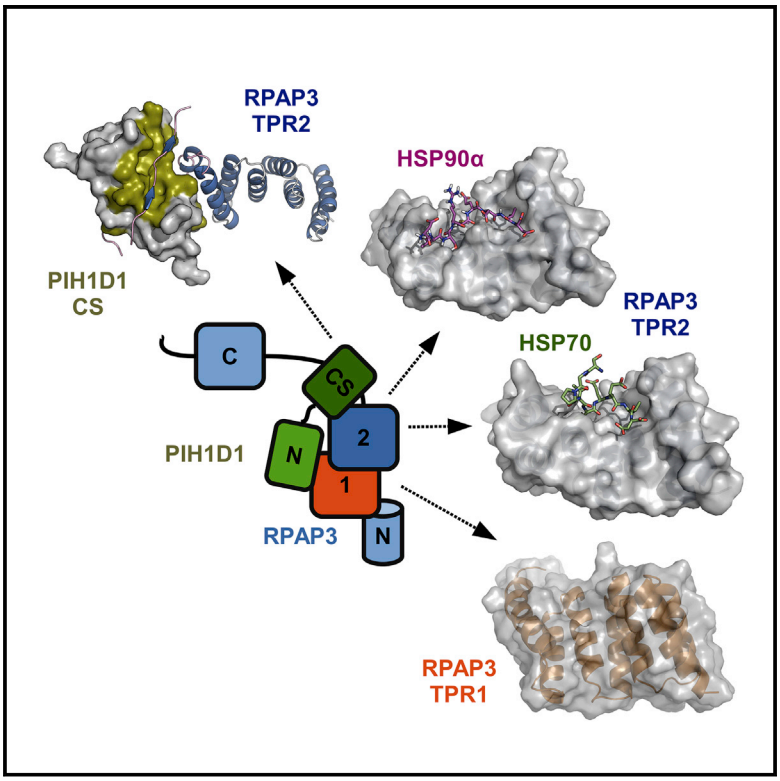

Highlights

- The TPR2 domain in RPAP3 is responsible for the recruitment of HSP90
- N-terminal domain in RPAP3 participates to the positive regulation of HSP90
- Isoform 1, and not isoform 2, of RPAP3 enlaces the CS domain of PIH1D1
- A R2T complex, involving RUVBL proteins and RPAP3 but not PIH1D1, exists *in vivo*

Authors

Julien Henri, Marie-Eve Chagot, Maxime Bourguet, ..., Sarah Cianférani, Xavier Manival, Marc Quinternet

Correspondence

philippe.meyer@ibpc.fr (P.M.), sarah.cianferani@unistra.fr (S.C.), xavier.manival@univ-lorraine.fr (X.M.), marc.quinternet@univ-lorraine.fr (M.Q.)

In Brief

Henri et al. highlight the structural features that permit to RPAP3 to strongly bind the C-terminal tail of HSP90 and the CS domain of PIH1D1. They proposed models, including HSP70, in which dimerization of RPAP3 is required for activation of HSP90.

Henri et al., 2018, Structure *26*, 1196–1209
September 4, 2018
https://doi.org/10.1016/j.str.2018.06.002

CellPress

CellPress

Structure
Article

Deep Structural Analysis of RPAP3 and PIH1D1, Two Components of the HSP90 Co-chaperone R2TP Complex

Julien Henri,[1,8] Marie-Eve Chagot,[2,8] Maxime Bourguet,[3,8] Yoann Abel,[4] Guillaume Terral,[3] Chloé Maurizy,[4] Christelle Aigueperse,[2] Florian Georgescauld,[1] Franck Vandermoere,[5] Rénette Saint-Fort,[1] Isabelle Behm-Ansmant,[2] Bruno Charpentier,[2] Bérengère Pradet-Balade,[6] Céline Verheggen,[4] Edouard Bertrand,[4] Philippe Meyer,[1,*] Sarah Cianférani,[3,*] Xavier Manival,[2,*] and Marc Quinternet[7,9,*]

[1]LBMCE, UMR 8226 CNRS Sorbonne Université, IBPC, 75005 Paris, France
[2]Université de Lorraine, CNRS, IMoPA, 54000 Nancy, France
[3]LSMBO, UMR 7178 CNRS Université de Strasbourg, IPHC, 67000 Strasbourg, France
[4]IGMM, UMR 5535 CNRS Université de Montpellier, Equipe Labellisée Ligue Contre le Cancer, 34293 Montpellier, France
[5]IGF, CNRS, INSERM, Université de Montpellier, 34094 Montpellier, France
[6]CRMB, UMR 5237 CNRS Université Montpellier, 34000 Montpellier, France
[7]Université de Lorraine, CNRS, INSERM, IBSLor, 54000 Nancy, France
[8]These authors contributed equally
[9]Lead Contact
*Correspondence: philippe.meyer@ibpc.fr (P.M.), sarah.cianferani@unistra.fr (S.C.), xavier.manival@univ-lorraine.fr (X.M.), marc.quinternet@univ-lorraine.fr (M.Q.)
https://doi.org/10.1016/j.str.2018.06.002

SUMMARY

RPAP3 and PIH1D1 are part of the HSP90 co-chaperone R2TP complex involved in the assembly process of many molecular machines. In this study, we performed a deep structural investigation of the HSP binding abilities of the two TPR domains of RPAP3. We combined 3D NMR, non-denaturing MS, and ITC techniques with Y2H, IP-LUMIER, FRET, and ATPase activity assays and explain the fundamental role played by the second TPR domain of RPAP3 in the specific recruitment of HSP90. We also established the 3D structure of an RPAP3:PIH1D1 sub-complex demonstrating the need for a 34-residue insertion, specific of RPAP3 isoform 1, for the tight binding of PIH1D1. We also confirm the existence of a complex lacking PIH1D1 in human cells (R2T), which shows differential binding to certain clients. These results highlight similarities and differences between the yeast and human R2TP complexes, and document the diversification of this family of co-chaperone complexes in human.

INTRODUCTION

HSP70 (70-kDa heat-shock protein) and HSP90 (90-kDa heat-shock protein) are highly conserved, ubiquitous, abundant, and essential molecular chaperones. The organization of HSP70/90 requires a complement of 20 co-chaperones to provide client specificity and to regulate activity. HSP70 binds denatured, misfolded, or aggregated proteins that display stretches of exposed hydrophobic amino acids and is involved in their early-stage folding (Jackson, 2013). HSP90 client proteins are often in near-native conformations and the chaperone is specialized in late-stage folding (Jackson, 2013). Most mammalian cells express two cytosolic isoforms of HSP90, HSP90α, and HSP90β, which are respectively, inducibly, and constitutively expressed.

The HSP90 molecular machine is a high-affinity and flexible homodimer and each monomer includes three structural domains (Shiau et al., 2006). The N-terminal domain, which contains the ATP binding site and binds co-chaperones, is followed by an intrinsically disordered variable charged linker. The middle domain encompasses a catalytic arginine required for ATPase activity and a client-protein binding site. The C-terminal domain includes a dimerization interface to make HSP90 an active-constitutive dimer with an extended V-shaped conformation. At its C terminus, the domain also contains a highly conserved MEEVD motif interacting with TPR-containing co-chaperones such as HOP/Sti1 and RPAP3/Tah1. Its biological activity, i.e., activation of client-protein, depends on the nucleotide status of its ATP binding site and the huge conformational changes in its three domains (Shiau et al., 2006). In addition, the activation specificity of HSP90 clients relies on interaction with its co-chaperones, which facilitates (or not) the progression through the different stages of the complex ATP hydrolysis cycle of the HSP90 molecular machine (Prodromou et al., 1999; Siligardi et al., 2004). In sum, this cycle involves the succession of at least two distinct extreme states. The HSP90 homodimer changes from an open V-like conformation to a compact closed one in which the two N-terminal domains interact under the direct control of ATP binding (Prodromou et al., 1999; Siligardi et al., 2004). Interestingly, by interacting with one C-terminal MEEVD motif, one HOP molecule was sufficient to stabilize the open conformation and fully inhibit the ATPase activity of HSP90 (Li et al., 2011). This leaves the second C-terminal MEEVD motif available for the binding of another co-chaperone. This implies that asymmetric complexes of HSP90 with two different TPR proteins are preferentially formed as intermediates *in vivo* and *in vitro* (Li et al., 2011). To complete the transition from the asymmetric HOP complex to the late-closed complex, the concerted binding of the ATP and the co-chaperone p23 is required. Finally, the

hydrolysis of ATP allows the release of the folded client-protein from HSP90.

The R2TP complex is conserved from yeast to human and appears specialized in the assembly of protein and RNP complexes (Rivera-Calzada et al., 2017; Tian et al., 2017; Zhao and Houry, 2005). It is involved in many cellular processes like small nucleolar ribonucleoprotein (snoRNP) biogenesis (Boulon et al., 2008), RNA polymerase (Boulon et al., 2010) or PIKK signaling (Horejsi et al., 2014). More in details, it composed of four different proteins: RUVBL1/Rvb1, RUVBL2/Rvb2, PIH1D1/Pih1, and RPAP3/Tah1 (human/yeast). RUVBL1/Rvb1 and RUVBL2/Rvb2 belong to the AAA+ family of ATPases and their relevant biologically arrangement appears to be an alternating hetero-hexamer/dodecamer. They have been proposed to themselves have chaperone activities (Tosi et al., 2013). PIH1D1/Pih1 and RPAP3/Tah1 heteromerize and are believed to function as an adapter to recruit clients, as well as bridge between HSP90 and the RUVBLs. Structural studies highlighted the C-terminal domain of RPAP3 as the recruiting module for RUVBLs in the human R2TP complex (Maurizy et al., 2018; Martino et al., 2018). In mammals, the R2TP further associates with a set of prefoldin proteins, which together form the PAQosome (Houry et al., 2018).

In yeast, the N-terminal part of Tah1 (1–91) encompasses a short atypical TPR domain that specifically recognizes the Hsp82 MEEVD motif, while its short disordered end (92–111) folds upon Pih1 binding (Back et al., 2013; Quinternet et al., 2015). *In vivo*, Tah1 stabilizes Pih1, which degrades alone, and initiates the formation of the R2TP complex (Zhao et al., 2008). Tah1, alone and in complex with Pih1, bridges Hsp82 up to a stoichiometric ratio of 2:2 (Eckert et al., 2010). In human, RPAP3 is a much larger protein comprising of 665 amino acids with two TPR domains, which may bind not only to HSP90 but also HSP70 (Benbahouche Nel et al., 2014). Interestingly, RPAP3 exhibits at least two splicing variants (iso): iso1 encompasses 34 more amino acids than iso2 and associates and stabilizes PIH1D1 (Yoshida et al., 2013). Structural basis for this specific binding is unknown, as well as the function of iso2 and complexes that it forms *in vivo*.

PIH1D1/Pih1 encompasses two domains (PIH1-N and PIH1-C). The PIH1-N region is a phospho-peptide binding domain which binds DpSDD/E consensus sites (Horejsi et al., 2014; Pal et al., 2014). PIH1-C is a CS domain, a motif found in several HSP90/Hsp82 co-chaperones, and is required for Tah1 and RPAP3 binding (Horejsi et al., 2014; Pal et al., 2014). In yeast, the Pih1:Tah1 heterodimer presents an inhibitory effect on the Hsp82 ATPase activity, and this could facilitate loading of client proteins to the chaperone (Eckert et al., 2010).

Here, we investigated the interaction between components of the human HSPs-R2TP complex, HSP90, HSP70, RPAP3, and PIH1D1 by using *in vitro* and *in vivo* experiments. First, we show that HSP90 is primarily recruited by the second TPR domain of RPAP3 and provide the structural determinants responsible for this specificity. We also show that the dimeric HSP90 was able to bind up to two RPAP3 molecules. Second, we examined the co-chaperoning of RPAP3 toward HSP90 and deciphered the stimulating and stabilizing effects of RPAP3. Finally, we identify the minimal binding sites between PIH1D1 and RPAP3 and solve the X-ray structure of this complex. This structure explains why RPAP3 iso2 does not strongly bind PIH1D1 and forms an unusual R2T complex *in vivo*.

RESULTS

The Two TPR Domains of Human RPAP3 Display Significantly Different Affinities for HSP Peptides

Human RPAP3 displays two TPR domains. TPR1 ($RPAP3_{133-255}$) and TPR2 ($RPAP3_{281-396}$) are both made of 7 α helices, and they both hold a carboxylate clamp that binds the last four EEVD residues of HSPs (Chagot et al., 2015). We designed one short ($M_{828}EEVD_{832}$) and two long (i.e., HSP90α or $D_{824}TSRMEEVD_{832}$ and HSP90β or $D_{824}ASRMEEVD_{832}$) HSP90 peptides as well as one HSP70 peptide ($S_{638}GPTIEEVD_{646}$) and took advantage of nuclear magnetic resonance (NMR) and non-denaturing mass spectrometry (MS) to determine both affinity and the binding region of these synthetic peptides toward the TPR of RPAP3.

For RPAP3-TPR1, we showed that the K_d values measured by NMR for the three different HSP90 peptides were around 100 μM. Significant chemical shift perturbations (CSPs) were observed in α helices 1, 3, and 5, which hold the carboxylate-clamp residues (Figures 1A–1C). With K_d values of around 35 μM, non-denaturing MS analysis performed with long HSP90 peptides are in agreement with the results of NMR (Figure S1).

For RPAP3-TPR2, we showed that the affinities measured with NMR for long HSP90 peptides were 20 times better, with K_d values of around 5 μM, than those obtained with RPAP3-TPR1 (Figures 1A–1C). Here again, with K_d values of around 10 μM, non-denaturing MS analysis confirmed increased affinities of RPAP3-TPR2 for long HSP90 peptides compared with RPAP3-TPR1 (Figure S1). We also observed that isoforms α and β of HSP90 did not display significant differences in terms of affinity for $RPAP3_{281-396}$. Interestingly, the short MEEVD peptide displayed a higher K_d of 131 μM for RPAP3-TPR2 and did not significantly affect α helix 7, unlike the long HSP90 peptides, which did. This suggests that residues before the MEEVD motif of HSP90 as well as the α helix 7 of RPAP3-TPR2 are key determinants for strong specific binding.

We inspected the HSP70 binding ability of RPAP3 using the same methods. The two TPR domains bound the HSP70 peptide with the same medium affinity (K_d values of around 50 and 30 μM for NMR and MS analyses, respectively; Figures 1D and S1). Nonetheless the CSP profiles differed significantly. For RPAP3-TPR1, the profile was very close to those obtained with all HSP90 peptides. For RPAP3-TPR2, here again, α helix 7 was perturbed upon peptide binding, in addition to α helices 1, 3, and 5. We observed that Ile642 in the SGPTIEEVD sequence provides more affinity than that obtained with the MEEVD peptide on both TPRs, but without reaching the K_d values recorded on RPAP3-TPR2 with long HSP90 peptides. Altogether, this suggests (1) that the way HSP70 binds to the two TPR could differ but that the subtle differences in the primary sequence of the two TPR lead to the same affinity and (2), that residue Ile642 from HSP70 could be involved.

This study of isolated TPR in particular draws attention to the second TPR domain of RPAP3 since it exhibits strong affinity for HSP90 peptides and CSPs specific to each peptide sequence. This contrasts with the first TPR domain of RPAP3 which

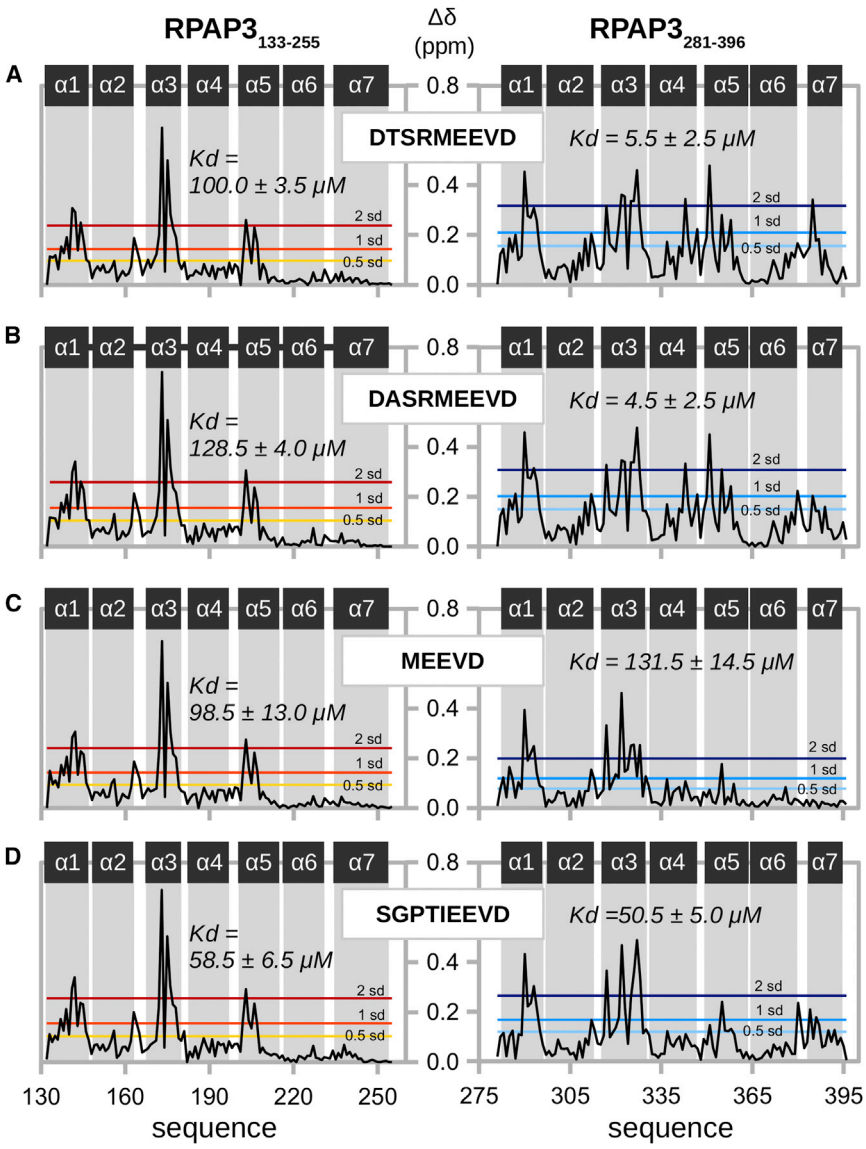

Figure 1. Interaction Analysis of Isolated TPR Domains from Human RPAP3 with HSP Peptides Using NMR

Backbone ^{1}H-^{15}N CSPs (Δδ expressed in ppm) of isolated TPRs are plotted against the sequence number (left, RPAP3-TPR1; right, RPAP3-TPR2). Values corresponding to 0.5, 1, and 2 SD are indicated with lines. K_d values deriving from Δδ are indicated. (A) to (D) present the analysis performed with peptides DTSRMEEVD (HSP90α), DASRMEEVD (HSP90β), and MEEVD and SGPTIEEVD (HSP70). See also Figure S1.

produces similar experimental responses whatever the peptide tested, especially in terms of CSPs.

The NMR Structure of RPAP3$_{281-396}$:HSP90 Highlights the Role of the Helix α7 and the Upstream Residues of the EEVD Motif in High-Affinity Recognition

To assess the molecular determinants of HSP90 binding to RPAP3-TPR2, we solved the NMR structure of the RPAP3$_{281-396}$:HSP90α peptide complex (for statistics see Table 1).

Our structure revealed that the HSP90α peptide adopts an extended conformation that relies entirely on the concave face of RPAP3-TPR2 (which contains 7 α helices) to reach a buried surface area of 1,464 ± 23 Å^2 (Figures 2A and 2B). In more detail, the EEVD motif is locked by polar contacts involving the five expected residues of the TPR carboxylate clamp (K286, N290, N321, K351, and R355) but also the side chain of K328 (Figure 2C). Accordingly, tested mutants N321E and R355A of RPAP3-TPR2 lost their association with HSP90 in yeast 2-hybrid (Y2H) assays (Figure S2). In our structure, Val731 in HSP90α is trapped in a hydrophobic pocket formed by F293, K294, Y305, and M324 of RPAP3$_{281-396}$ (Figures 2C and 2D). Upstream of the HSP consensus sequence, Met728 is hosted in a cradle made by α helices 3 and 5 of the TPR domain and is stabilized by hydrophobic contacts with M324, L327, R355, and T358 in RPAP3-TPR2 (Figure 2D). Moreover, the side chain and backbone of Ser726 can establish hydrogen bonds with the side chains of E380 and K384, respectively. Interestingly, K384, which is held by helix α7 of RPAP3-TPR2, is also involved in polar interactions with the initial Asp724 of the peptide and its long side chain offers a favorable environment for hosting Thr725 against the α6-α7 loop (Figure 2E). Accordingly, mutants K384A and K384A-Q385A in RPAP3-TPR2 lost their association with HSP90 in Y2H assays (Figure S2).

These structural data on the RPAP3$_{281-396}$:HSP90α peptide complex reveal the marked influence of the four first residues of long HSP90 peptides in protein binding. The data are also in good agreement with previous CSP mapping and explain why the helix α7 of RPAP3-TPR2 is required for optimal affinity between HSP90 and its co-chaperone.

The NMR Structure of RPAP3$_{281-396}$:HSP70 Provides Data on the HSP Specificity of RPAP3

The binding of the HSP70 peptide promoted CSPs in helix α7 of RPAP3-TPR2, as observed for long HSP90 peptides. However, affinity for the SGPTIEEVD sequence was 10 times lower than that measured with the D(T/A)SRMEEVD sequences. To address this question, we solved the NMR structure of the RPAP3$_{281-396}$ in complex with HSP70 (Figure 2F; for statistics see Table 1).

As expected, the HSP70 peptide was again stabilized through polar contacts involving the EEVD motif and residues of the TPR carboxylate clamp added from the K328 side chain (Figure 2H). We noticed that K294 was seen to participate in this network by making contact with Glu644, while Val645 of the peptide is

Table 1. NMR-Derived Restraints and Structural Statistics for the 20 Best Structures of $RPAP3_{281-396}$ in Complex with HSP90α and HSP70 Peptides and of Free $RPAP3_{133-255}$

	$RPAP3_{281-396}$ HSP90α	$RPAP3_{281-396}$	HSP90α (DTSRMEEVD)	$RPAP3_{281-396}$ HSP70	$RPAP3_{281-396}$	HSP70 (SGPTIEEVD)	$RPAP3_{133-255}$
NMR Distances and Dihedral Constraints							
Distance constraints							
Total NOEs	2,900	2,690	59	3,637	3,378	96	2,589
Short range ($\|i-j\| \leq 1$)	1,307	1,253	54	1,517	1,434	83	1,185
Medium range ($\|i-j\| < 5$)	793	788	5	1,076	1,063	13	813
Long range ($\|i-j\| \geq 5$)	798	647	0	1,044	881	0	591
Intermolecular NOEs	151			163			
Total dihedral angle restraints	199	199	0	199	199	0	216
Φ	98	98	0	100	100	0	109
Ψ	99	99	0	99	99	0	107
Structure Statistics							
Violation occurrences							
Distance constraints (>0.5 Å)	0	0	0	0	0	0	0
Dihedral angle constraints (>5°)	0	0	0	0.1 ± 0.3	0.1 ± 0.3	0	0.2 ± 0.4
Deviations from idealized geometry							
Bond lengths ($\times 10^{-3}$ Å)	3.239 ± 0.113						
Bond angles (°)	0.468 ± 0.015						
Impropers (°)	1.265 ± 0.054						
RMSD to best structure (Å)	resi. 281 to 394 + 724 to 732	resi. 281 to 394	resi. 724 to 732	resi. 281 to 394 + 640 to 646	resi. 281 to 394	resi. 640 to 646	resi. 133 to 251
Backbone atoms	0.36 ± 0.04	0.33 ± 0.05	0.51 ± 0.13	0.28 ± 0.04	0.26 ± 0.04	0.43 ± 0.11	0.39 ± 0.07
Heavy atoms	0.64 ± 0.04	0.58 ± 0.05	1.07 ± 0.24	0.53 ± 0.06	0.49 ± 0.05	0.90 ± 0.31	0.65 ± 0.07
Ramachandran statistics (%)							
Residues in most favored regions	89.5			92.0			90.5
Residues in additional allowed regions	10.5			8.0			9.4
Residues in generously allowed regions	0			0			0.1
Residues in disallowed regions	0			0			0
Surface ($Å^2$)	7,189 ± 79	7,190 ± 69	1,463 ± 25	7,220 ± 74	7,115 ± 52	1,262 ± 51	7,612 ± 76
Buried surface area ($Å^2$)	1,464 ± 23			1,157 ± 27			

NOEs, nuclear Overhauser effects; RMSD, root-mean-square deviation; resi., residues.

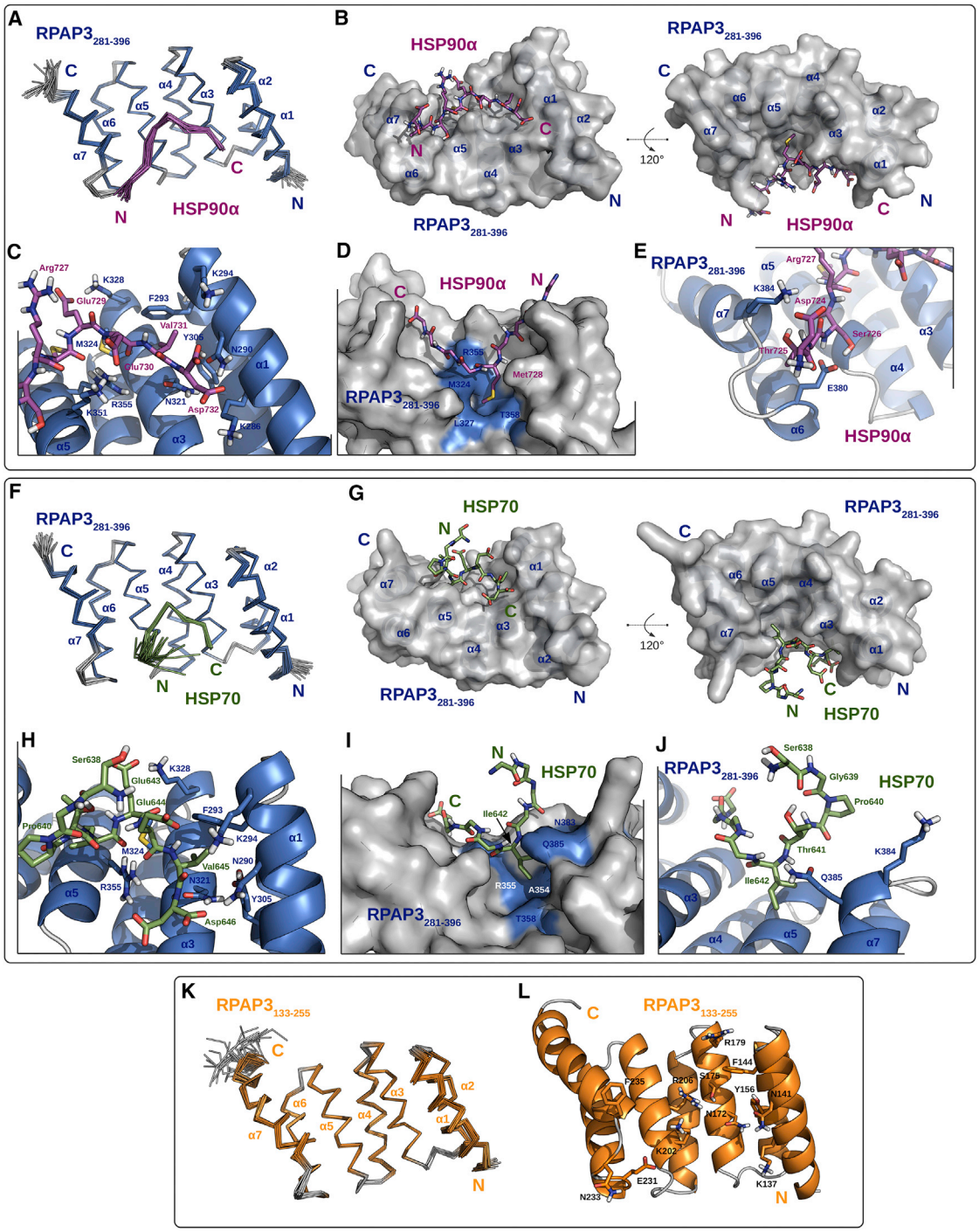

Figure 2. NMR Structures of the Complexes between RPAP3$_{281-396}$ and HSP Peptides and of Free RPAP3$_{133-255}$

(A, F, and K) Backbone trace of the top 20 NMR structures.

(B and G) Two views of the best NMR structure. HSP peptides are represented as sticks and the molecular surface of RPAP3$_{281-396}$ is in gray.

(C and H) Zoom on the carboxylate-clamp region.

(D and I) Zoom on the binding pocket of RPAP3 hosting Met728 of HSP90α or Ile642 of HSP70.

(E and J) Zoom on the region of the helix α7 from RPAP3$_{281-396}$. From (C to E) and (G to J), the best NMR structures were used.

(L) Stick representation of key residues in RPAP3$_{133-255}$ using the best NMR structure. Only polar hydrogens are represented.

See also Figure S2.

hosted in the same hydrophobic pocket as the one determined for Val731 of HSP90α (Figure 2H). However, differences were observed in the conformation of residues upstream of the EEVD motif of HSP70. First, Ile642 in HSP70 is positioned with respect to α helices 5 and 7 (and not helices 3 and 5 as observed for Met728 of HSP90α) of the TPR domain (Figures 2G, 2I, and 2J) but A354, R355, T358, N383, and Q385 in RPAP3 do not *a priori* represent a favorable environment for a bulky hydrophobic side chain (Figure 2I). Even so, a hydrogen-bond was observed between the Ile642 and Q385 backbones (Figure 2J). This "by-default" region of RPAP3 appears to be the only one with enough room to accept the Ile residue. In comparison, the corresponding Met728 in HSP90 penetrates deeper into the TPR structure, which should enhance its stability. Second, the HSP70 peptide covers less of the protein than the area covered by HSP90α (buried surface area of 1,157 ± 27 $Å^2$ compared with 1,464 ± 23 $Å^2$ for HSP90; Figures 2G, 2I, and 2J). Indeed, Pro640 induces a turn in the peptide and Ser638 and Gly639 are ejected from the TPR structure (Figure 2J). Thus, the latter residues are not placed against, but are simply in the neighborhood of the α6-α7 loop of RPAP3. Consequently, K384 does not play the same stabilizing role as for HSP90α.

Thus, the NMR structure of $RPAP3_{281-396}$:HSP70 is in agreement with the previously recorded CSPs and also explains why the second TPR of RPAP3 has more affinity with long HSP90 peptides.

$RPAP3_{133-255}$ Does Not Possess the Structural Keys Required for Strong Binding of HSP Peptides

To complete our structural study, we obtained the NMR structure for the free form of RPAP3-TPR1, with the aim of identifying the structural features that could be responsible for its lower affinity for HSP peptides (for statistics see Table 1).

As expected, $RPAP3_{133-255}$ is organized in a succession of 7 α helices (Figure 2K) and nicely superimposes with $RPAP3_{281-396}$ (Cα root-mean-square deviation [RMSD] = 0.9 Å). Residues forming the carboxylate clamp (K137, N141, N172, K202, and R206) are in a favorable position for peptide binding (Figure 2L).

The previous CSP experiments recorded with HSP70/90 peptides and RPAP3-TPR1 supported the idea that only the EEVD motif is responsible for binding. Indeed, long or short HSP90 as well as HSP70 peptides lead to very similar maps on RPAP3-TPR1, in which only α helices 1, 3, and 5 are affected upon binding (Figures 1A–1C). This strongly suggests that the N-terminal sequence D(T/A)SR or SGPT sequences of HSP90/70 peptides are rejected toward the solvent in the complex formed with RPAP3-TPR1. Interestingly, even if the α6-α7 loop is quite well conserved between TPR1 and TPR2 of RPAP3, a polar substitution can be seen in RPAP3-TPR1 compared with RPAP3-TPR2 (N233 to G382), which could hinder stabilization of the T/A methyl group in HSP90 (Figure 2L). Moreover, at the root of helix α7, K384, which is important in TPR2 is replaced by F235 in TPR1 and can thus not ensure its role in stabilizing the N-terminal part of the peptide (Figure 2L).

The Second TPR Domain of RPAP3 Is Dedicated to Initial Binding of HSP90

The results of our analysis of isolated TPR domains of RPAP3 were strongly in favor of a preference of HSP90 for RPAP3-TPR2. To confirm this hypothesis, we verified the binding of the peptides in presence of the two TPRs. We benefited from the unique feature of NMR to monitor the binding of a ligand on its target at the atomic level and monitored the ^{1}H-^{15}N HSQC NMR spectrum of $RPAP3_{133-396}$ with increasing amounts of HSP90α. Amide correlations were used as probes of each TPR domain inside the tandem $RPAP3_{133-396}$. For example, G347, which belongs to TPR2, behaved in exactly the same way in $RPAP3_{281-396}$ and in $RPAP3_{133-396}$, with instantaneous and rapid displacement along the spectrum upon addition of the peptide (Figures 3A–3C). In contrast, S175, which belongs to TPR1, showed a delay in displacement when tracked in $RPAP3_{133-396}$ compared with in $RPAP3_{133-255}$ (Figures 3D–3F). Moreover, as the trajectories of amide peaks remained linear in the ^{1}H-^{15}N spectra, we concluded that the two HSP90 binding sites within $RPAP3_{133-396}$ were independent and not influenced by one another. With this NMR titration experiment, we unambiguously showed that the "high-affinity" TPR2 in $RPAP3_{133-396}$ started pumping the ligand, which is not immediately available for the "low-affinity" TPR1. The same NMR approach applied to $RPAP3_{133-396}$ and the HSP70 peptide did not display a "ligand pumping" effect (Figure S3). This highlights the very similar affinities of the two TPR domains for the HSP70 peptide.

Dimeric HSP90 Can Bind up to Two RPAP3

Based on our previous results, we focused on the interaction between RPAP3 and HSP90 with the aim of determining the stoichiometry of the interaction using non-denaturing MS experiments. Since mass spectra recorded with the free full-length RPAP3 were unfortunately of poor quality (data not shown), we used $RPAP3_{133-396}$.

Figure 3G presents the non-denaturing mass spectra obtained in presence of 20 μM of full-length HSP90 and increasing amounts of $RPAP3_{133-396}$. In absence of $RPAP3_{133-396}$, a charge state distribution was detected with a measured mass of 169,737 ± 14 Da corresponding to dimeric HSP90 (green peaks). In presence of 5 μM of $RPAP3_{133-396}$ (0.5 molar equivalent of TPR per HSP90 monomer), signal corresponding to 2:1 HSP90:$RPAP3_{133-396}$ complex (orange peaks) was detected along with dimeric HSP90. When the amount of $RPAP3_{133-396}$ complex was increased to 10 μM (1 molar equivalent of TPR per HSP90 monomer), an additional ion series corresponding to the binding of two $RPAP3_{133-396}$ appeared (magenta peaks), which became the most intense ion series at higher concentrations of $RPAP3_{133-396}$, demonstrating the ability of the full-length HSP90 to bind up to two $RPAP3_{133-396}$. In the light of our data, this first suggests a model in which the two MEEVD motifs of the dimeric HSP90 were each bound to one RPAP3 via its TPR2.

These data, strengthened by additional MS and isothermal titration calorimetry (ITC) analysis (Figure S3), demonstrate that HSP90 is a preferential partner of RPAP3, and that this likely occurs via its TPR2. We aimed to validate these data *in vivo* first using quantitative pairwise IP-LUMIER (immunoprecipitation-luminescence-based mammalian interactome mapping) assays (Figure 4A). As expected, we showed a better association of HSP90 with isolated RPAP3-TPR2 than with isolated RPAP3-TPR1, suggesting that TPR2 in the full-length or tandem RPAP3 is responsible for the major part of the IP efficiency

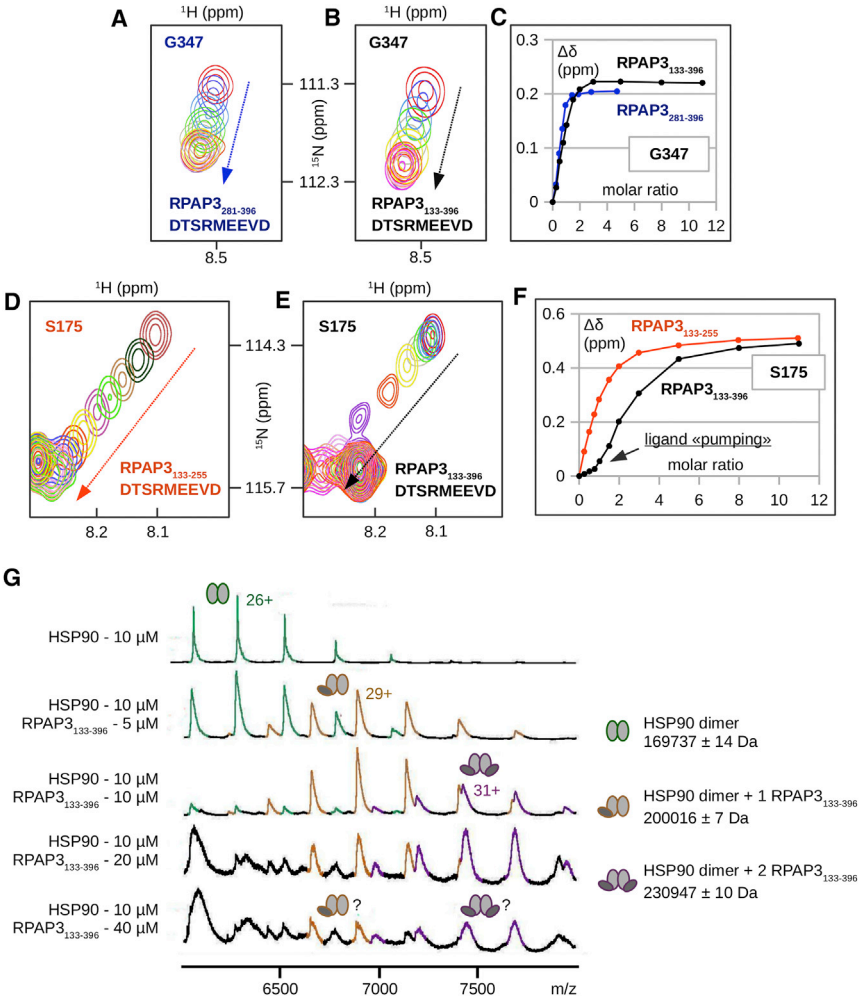

Figure 3. Analysis of RPAP$_{133-396}$ in Complex with HSP Peptides and Full-Length HSP90

(A, B, D, and E) Chemical shift perturbations of the ^{1}H-^{15}N correlation peak upon HSP90α peptide binding for G347 in RPAP3$_{281-396}$ (A) and in RPAP3$_{133-396}$ (B), as well as for S175 in RPAP3$_{281-396}$ (D) and in RPAP3$_{133-396}$ (E).

(C and F) Δδ for G347 and S175 are plotted against the molar ratio between peptide and protein (C and F).

(G) Determination of the binding stoichiometry between RPAP3$_{133-396}$ and full-length HSP90 (G). RPAP3$_{133-396}$ and HSP90 are respectively represented by dark and light gray oval forms. Green, orange, and magenta peaks on mass spectra correspond respectively to HSP90 dimer, HSP90 dimer +1 tandem TPR and HSP90 dimer +2 tandems TPR.

See also Figure S3.

obtained toward HSP90. Having confirmed the importance of the TPR2 in HSP90 recruitment, we then wished to determine the *in vivo* partners of RPAP3-TPR1 using proteomic analysis. We created a stable HeLa cell line expressing a GFP-TPR1 fusion and performed a stable isotope labeling with amino acids in cell culture (SILAC) IP using anti-GFP antibodies (Figure 4B). Interestingly, we showed that isolated RPAP3-TPR1 associated *in vivo* with HSP70's family protein (HSPA4, HSPA6, HSPA8, HSPA1B, and HSPA4L) whereas HSP90 was absent of the SILAC IP analysis. This suggests that RPAP3 could recruit both HSP70 and HSP90 through its two TPR domains, sequentially or at the same time.

RPAP3 Actively Regulates the HSP90 Chaperone Cycle

The HSP90 chaperone function relies strictly on conformational cycling through adenosine nucleotide binding, hydrolysis and release (Panaretou et al., 1999). We assayed the effect of human RPAP3 on the ATPase cycle of HSP90. Full-length RPAP3 stimulated HSP90 ATPase 1.8-fold (Figure 5A), demonstrating that RPAP3 is an active co-chaperone of HSP90. This observation is consistent with yeast HSP90 stimulation by Tah1 (Eckert et al., 2010) and *Drosophila melanogaster* stimulation of Hsp83 by Spaghetti (Benbahouche Nel et al., 2014) and supports a conserved function of Tah1/Spagh/RPAP3 function in the eukaryotic lineages.

Since RPAP3 displays two independent anchoring EEVD sites, we compared the co-chaperone stimulation with mutants of each TPR (N172D for TPR1 or N321D for TPR2). Mutation of TPR2 caused complete loss of stimulation while mutation of TPR1 had no significant effect on HSP90 ATPase stimulation (Figure 5A). Hence, HSP90 carboxy-peptide single anchoring at TPR2 is necessary and sufficient for RPAP3 regulation of the HSP90 cycle.

HSP90-NTD homodimerizes upon ATP binding and middle domain K380 in yeast contacts ATP γ-phosphate, licensing the active site for catalysis (Meyer et al., 2003). Yeast K380 loop is released by interaction with the amino-terminal domain (1–153) of yAha1 (Meyer et al., 2004). We assayed the stimulation effect of RPAP3 in the presence of yAha1$_N$. In the presence of 100 μM of yAha1$_N$ the activity of HSP90 was stimulated 5-fold (data not shown). Further addition of RPAP3 caused an additional 2.5-fold stimulation (Figure 5A), demonstrating that regulation of the ATPase by RPAP3 targets a step distinct from that of yAha1$_N$.

RPAP3$_{133-396}$ caused no measurable stimulation of HSP90 ATPase (Figure 5A) whereas fragment 1–396 of RPAP3 was able to activate HSP90 in a manner similar to the full-length protein. This strongly suggests that the N-terminal region 1–132 of RPAP3 (RPAP3-NTD) is required for HSP90 stimulation. We then produced and purified fragment 1–132 of RPAP3. This domain forms soluble aggregates, in agreement with the strong coiled-coil propensity found in this region of RPAP3 (Figure S4). Analysis of gel filtration profiles revealed that the full-length RPAP3 as well as fragment 1–396 could be multimeric (Figure S4), whereas RPAP3$_{133-396}$ behaved as a monomer (as demonstrated by NMR and ITC). Altogether, it suggests that

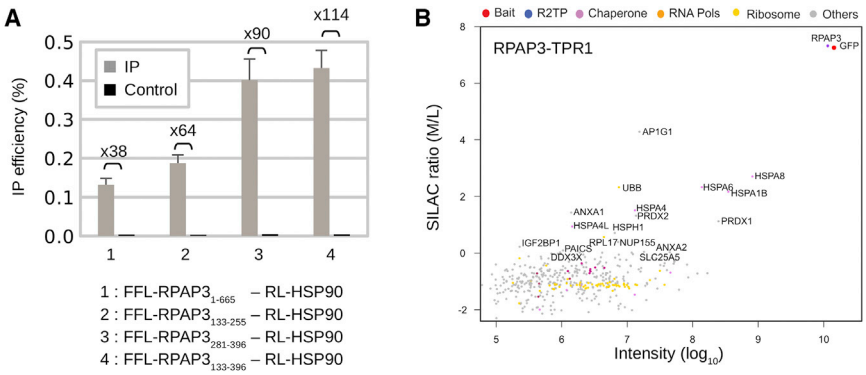

Figure 4. IP-LUMIER Assays between RPAP3 and HSP90 and SILAC IP of RPAP3-TPR1

(A) RPAP3 and HSP90 were respectively fused to Firefly luciferase (FFL) and to Renilla luciferase (RL). IP efficiency (mean ± SD) and fold value (IP versus control) are indicated.

(B) SILAC ratios (y axis) as a function of signal abundance (x axis) measured by quantitative proteomic analysis of extracts from HeLa cells expressing GFP-RPAP3-TPR1 and immunoprecipitated with anti-GFP antibody. SILAC ratios were calculated from a control IP done with parental HeLa cells. Each dot represents a protein and is color coded. Significance values are listed in Table S1.

dimerization/multimerization of RPAP3 via its N-terminal part could be crucial for HSP90 regulation.

HSP90 dimerizes at its C-terminal domain, with a dynamic exchange of dimer subunits (Retzlaff et al., 2010). Using the same fluorescence resonance energy transfer (FRET) subunit exchange rate assay (Figure 5B), we measured an yHSP90 dimer half-life of 52 s. When incubated with the full-length RPAP3 or fragment 1–396, the dimer half-life significantly increased by ~2-fold (Figure 5C). In contrast, $RPAP3_{133-396}$ caused no stabilization of the yHSP90 dimer. Hence, yHSP90 dimer stabilization by RPAP3 correlates with ATPase stimulation. Here again, the RPAP3-NTD seems to play a role in this stabilization.

Taken together, these results suggest that RPAP3 interacts primarily with HSP90 at the TPR2 clamp, forming an HSP90:RPAP3 complex of 2:1 or 2:2 stoichiometries. RPAP3 allosterically stabilizes the dimeric ATPase-competent state of the chaperone, favoring closure of the HSP90-NTD in an active ATPase.

RPAP3 Iso1 Interacts Extensively with PIH1D1

Next, we focused on the interface between RPAP3 and PIH1D1, which has not been previously characterized. Interestingly, eviction of exon 12 in RPAP3 by alternative splicing leads to two protein isoforms. Iso1 is 34 residues longer than iso2 and the insertion is located downstream of the RPAP3-TPR2 (residues 396–429). Most importantly, previous IP experiments demonstrated the importance of this sequence for the binding of PIH1D1 (Yoshida et al., 2013). To understand the contribution of the 34-residues insertion in RPAP3 iso1, we conducted co-expression assays in *E. coli*. We showed that this 34 residues fragment was required for efficient binding of PIH1D1 and its C-terminal part (Figure S5). The results are in agreement with a pull-down assay demonstrating a direct interaction between GST-$RPAP3_{400-420}$ and the CS domain of PIH1D1 (Martino et al., 2018). Finally, using non-denaturing MS, we demonstrated that a stable complex suitable for structural studies could be obtained between fragments 281–445 of RPAP3 and 199–290 of PIH1D1 (Figure S6).

This complex was crystallized in 100 μm platelets of the C_2 space group (Table 2). Experimental electron density maps enabled modeling of polypeptides $RPAP3_{283-443}$ and $PIH1D1_{203-290}$. PIH1D1 folds as seven β strands that form a CS domain, whereas RPAP3 folds as four pairs of α helices, the seven firsts helices stacking into the canonical TPR fold of HSP co-chaperones (Figure 6A). Strikingly, the RPAP3 globular domain extends into a long arm (stretching from residue 409–443) that loops around PIH1D1 (Figure 6B). Unfortunately, due to a lack of electron density, region 425–429 could not have been reconstructed. As seen in the yeast complex (Pal et al., 2014; Quinternet et al., 2015), this RPAP3 arm encloses two β strands (segments 433–435 for strand β1 and 437–440

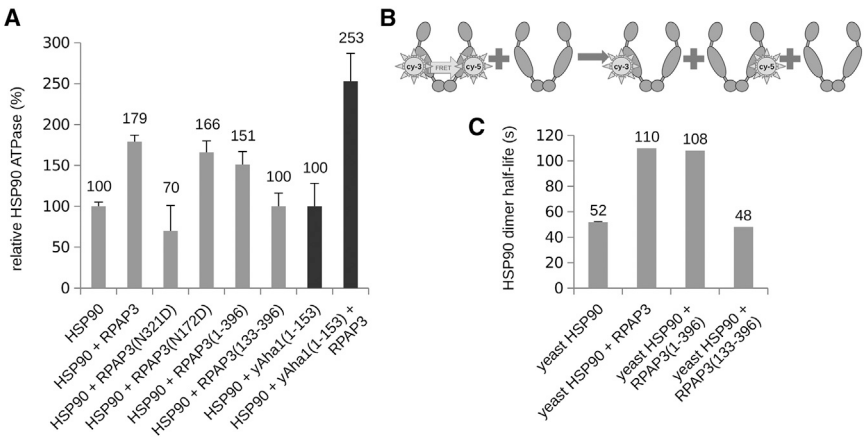

Figure 5. RPAP3 Co-chaperoning of HSP90 *In Vitro*

(A) Steady-state kinetic HSP90 ATPase at saturation of ATP was reported by PK-LDH and corrected with geldanamycin or radicicol against a specific signal. Relative activity is reported with respect to HSP90 alone (100%). Right: black bars, HSP90 reference and tested activities are stimulated 5-fold by 100 μM of *Saccharomyces cerevisiae* $Aha1_{1-153}$. Data are represented as means ± SD.

(B) Schematic principle of HSP90 dimer subunit exchange assay. HSP90 dimeric state was probed with FRET signal of hetero-labeled yeast (HSP90-mQ385C-cy3):(HSP90-mQ385C-cy5).

(C) Yeast HSP90 dimer half-life alone or in the presence RPAP3, $RPAP3_{1-396}$, or $RPAP3_{133-396}$. Error bar of yeast HSP90 alone represents a SD of 0.5 s over three replicates.

See also Figure S4.

Table 2. Data Collection and Refinement Statistics for $RPAP3_{281-445}$:$PIH1D1_{199-290}$ X-Ray Structure

	$RPAP3_{281-445}$:$PIH1D1_{199-290}$
Data Collection	
Space group	C 1 2 1
Cell dimensions	
a, *b*, *c* (Å)	135.98, 42.44, 112.71
α, β, γ (°)	90.0, 98.248, 90.0
Resolution (Å)	67.287–2.965 (3.071–2.965)[a]
R_{merge} (%)[b]	14.8 (90.9)
$I/\sigma I$	11.6 (2.2)
Completeness (%)	98.99 (99.26)
Multiplicity	7.0 (7.4)
Refinement	
Resolution (Å)	2.965
No. of reflections	13,468 (1,341)
R_{work}/R_{free}	0.2235 (0.3527)/0.2823 (0.4199)
No. of atoms	3,864
Protein	3,846
Ligand/ion	1
Water	17
Average B factors	56.07
Macromolecules	56.14
Ligands	57.01
Solvent	41.32
RMSD	
Bond lengths (Å)	0.004
Bond angles (°)	0.58
Ramachandran statistics (%)	
Favored	95.9
Allowed	4.09
Outliers	0.00
Buried surface area (Å^2)	>3,093

RMSD, root-mean-square deviation.
[a]Values in parentheses are for highest-resolution shell.
[b]$R_{merge} = S_{hkl}\, S_i\, |I_i(hkl) - (I(hkl))|/S_{hkl}\, S_i\, I_i(hkl)$, where $I_i(hkl)$ is the *i*th observation of reflection *hkl* and $<I(hkl)>$ is the weighted average intensity for all observations of reflection *hkl*.

for strand β2) which form intermolecular sheets with strands β3 and β6 of PIH1D1 (Figures 6A and 6B). In more detail, the terminal helices α7 and α8 in RPAP3 contact a hydrophobic patch on PIH1D1 strands β1, β2, β6, and β7 (Figure 6C). This interface is lined by polar contacts at RPAP3-S391:PIH1D1-D218, RPAP3-K394:PIH1D1-E215 and the 3-pronged polar contacts RPAP3-D404:PIH1D1-H273, R276 (Figure 6C). Segment 409–419 in RPAP3 extended peptide runs along a hydrophobic crevice delineated by PIH1D1 strands β1 and β5 (Figure 6B), RPAP3-V417 notably shielding L212 and L214 in PIH1D1 from solvent. Remarkably, RPAP3-I437 side chain dives into a hydrophobic pocket in PIH1D1 formed by A270, F272, A232, L235, and L237 (Figure 6D). Finally, a minimum of 3,093 Å^2 was protected from solvent, stabilizing the complex into a highly constrained orientation.

Internal mobility of the free form of $RPAP3_{281-445}$ was assessed by NMR through measurement of the backbone ^1H-^{15}N heteronuclear nuclear Overhauser effect ratios (Figure S7). The marked decrease in the ratios in the C-terminal part of $RPAP3_{281-445}$ (which starts after helix α7 and continues until position 445) demonstrates that the region of RPAP3 which is able to bind PIH1D1 is natively disordered. This is reminiscent of what was observed in the yeast Tah1 (Quinternet et al., 2015). Finally, ITC experiments showed that RPAP3-TPR2 kept the same binding properties toward HSP peptides in presence of PIH1D1 CS domain (Figure 6E).

The N-Terminal Domain in PIH1D1 Weakly Interacts with RPAP3-TPR1

To inspect a possible influence of the N-terminal phospho-binding domain in PIH1D1 (PIH1D1-N) on the interaction with RPAP3, we performed NMR titration experiments using fragment 1–180 of PIH1D1. We showed that addition of PIH1D1-N degraded specifically the NMR signal of ^{15}N-labeled RPAP3-TPR1 when taken in an isolated form or included in the tandem $RPAP3_{1-396}$. No significant variation of the NMR signal of RPAP3-TPR2 was observed upon addition of PIH1D1-N (Figure 6F).

Since co-expression assays failed between full-length PIH1D1 and isolated TPRs (Figure S5), these results suggest a low but real affinity of PIH1D1-N for RPAP3-TPR1. Interestingly, they suggest that secondary contacts between the two latter domains are set up after the locking of PIH1D1 CS domain into RPAP3 iso1.

Isoforms 1 and 2 of RPAP3 Coexist in Cells and Isoform 1 Is Required for Strong Direct Binding of PIH1D1

Finally, we performed experiments to analyze the functions of RPAP3 isoforms *in vivo*. Using RNA samples from different human cell lines, we analyzed the distribution of RPAP3 mRNA splicing isoforms by RT-PCR (Figure 7A). Iso1 was predominantly found in all the cell lines tested. The ratio iso1/iso2 increased in fibroblasts compared with cell lines derived from a variety of cancers (HeLa S3, Kato-III, and A549) or the adenovirus-transformed cell line HEK293. We expanded our investigation to test whether different stresses could also alter the relative abundance of RPAP3 splice isoforms. None of the stress conditions tested (heat shock, oxidative stress or ionizing radiations) drastically changed the balance between RPAP3 isoforms, even if heat stress caused a small (89.4–85.8) but significant ($p < 0.001$) decrease in the ratio iso1/iso2.

After having shown that both isoforms could co-exist in cells, we wanted to obtain a more complete landscape of their protein partners. To this end, we generated HeLa cell lines stably expressing GFP-RPAP3 iso1 and GFP-RPAP3 iso2, and performed SILAC proteomics using anti-GFP antibodies (Figures 7B–7D). We found that both isoforms associate with RUVBL1, RUVBL2, and several prefoldins, as well as with some clients and chaperone (HSPA1B, HSPA6, and BAG2). Other proteins appeared enriched for RPAP3 iso1, which included known clients of R2TP and their cofactors, such as POLR2A and RPAP2 for RNA polymerase II, and ZNHIT2, PRPF8, and EFTUD2 for U5 snoRNP. A few proteins appeared also highly specific for the

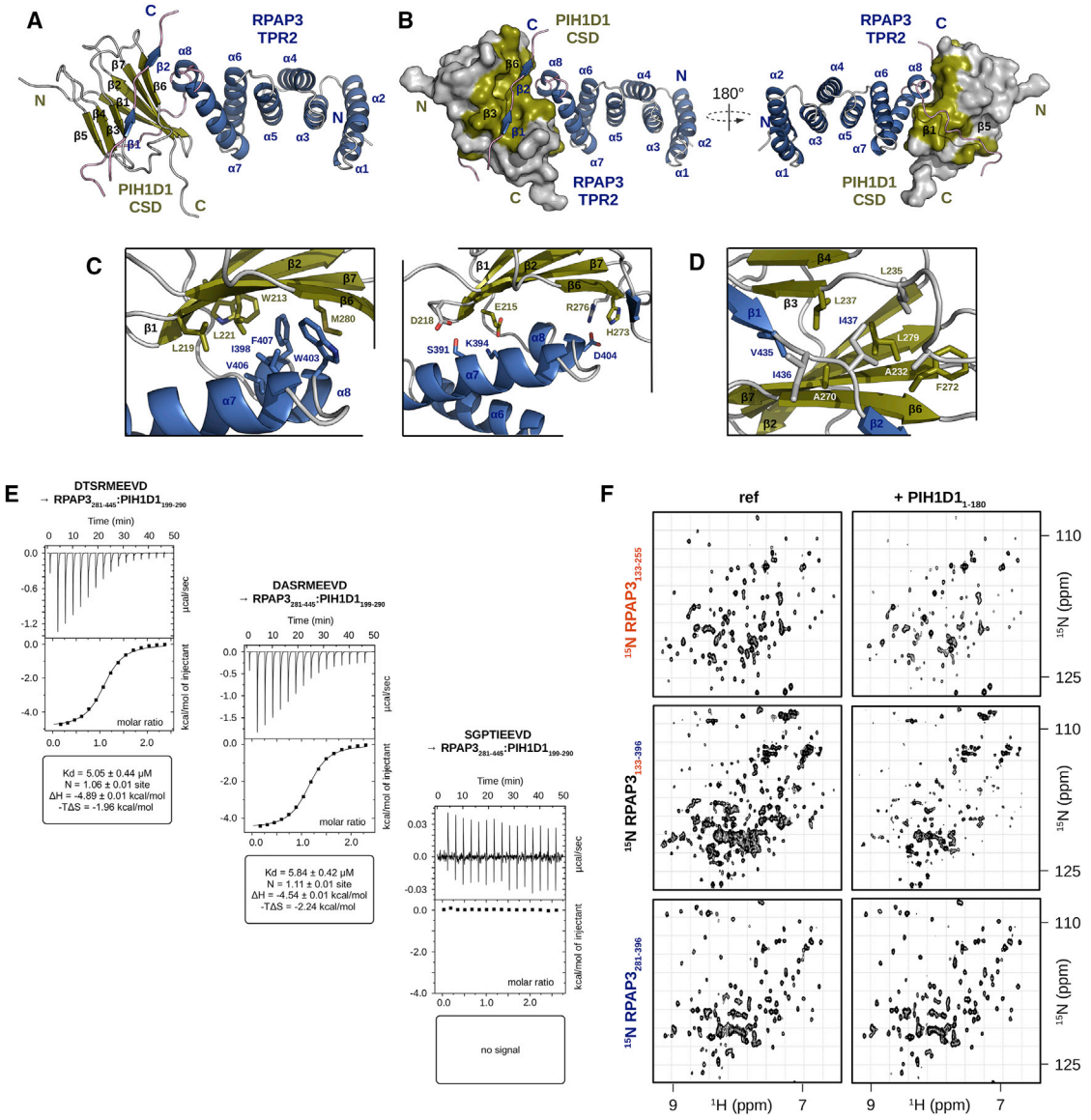

Figure 6. X-Ray Structure of the Complex RPAP3$_{281-445}$:PIH1D1$_{199-290}$

(A) Cartoon view of the complex. The CS domain of PIH1D1 (CSD) is in green, RPAP3-TPR2 is in blue and the segment 396–445 of RPAP3 is in pink.

(B) Two views of the complex in which the molecular surface of PIH1D1 is represented. The molecular surfaces of residues in PIH1D1 in the close proximity to RPAP3 are in green.

(C) Zoom on hydrophobic and polar contacts between residues that stabilize the regions of the helices α7 and α8 in RPAP3 and strands β1, β2, β6, and β7 in PIH1D1.

(D) Binding pocket of I437 in RPAP3.

(E) ITC experiments between RPAP3$_{281-445}$:PIH1D1$_{199-290}$ and HSP peptides.

(F) ^{1}H-^{15}N HSQC spectra of ^{15}N-labeled fragments 133–255, 133–396, and 281–396 of RPAP3 in absence (left column) or in presence (right column) of PIH1D1$_{1-180}$.

See also Figures S5–S8.

RPAP3 iso1 IP, which included the likely client SEC16A, some chaperones of the HSP90 and HSP70 families (HSP90AA1, HSP90AB1, and HSPA4), and PIH1D1 itself as expected. As for yeast proteins in which contacts were highlighted between Pih1 and HSP90 (Quinternet et al., 2015), SILAC IP experiments strongly suggests that PIH1D1 stabilizes the interaction between RPAP3 and HSP90. Only few proteins appeared more highly enriched in the RPAP3 iso2 IP. Taken together, these data demonstrate that RPAP3 iso1 forms the canonical R2TP complex, while RPAP3 iso2 forms a related complex lacking PIH1D1, and that is thus termed R2T. These complexes associate with a different set of proteins and might have different functions.

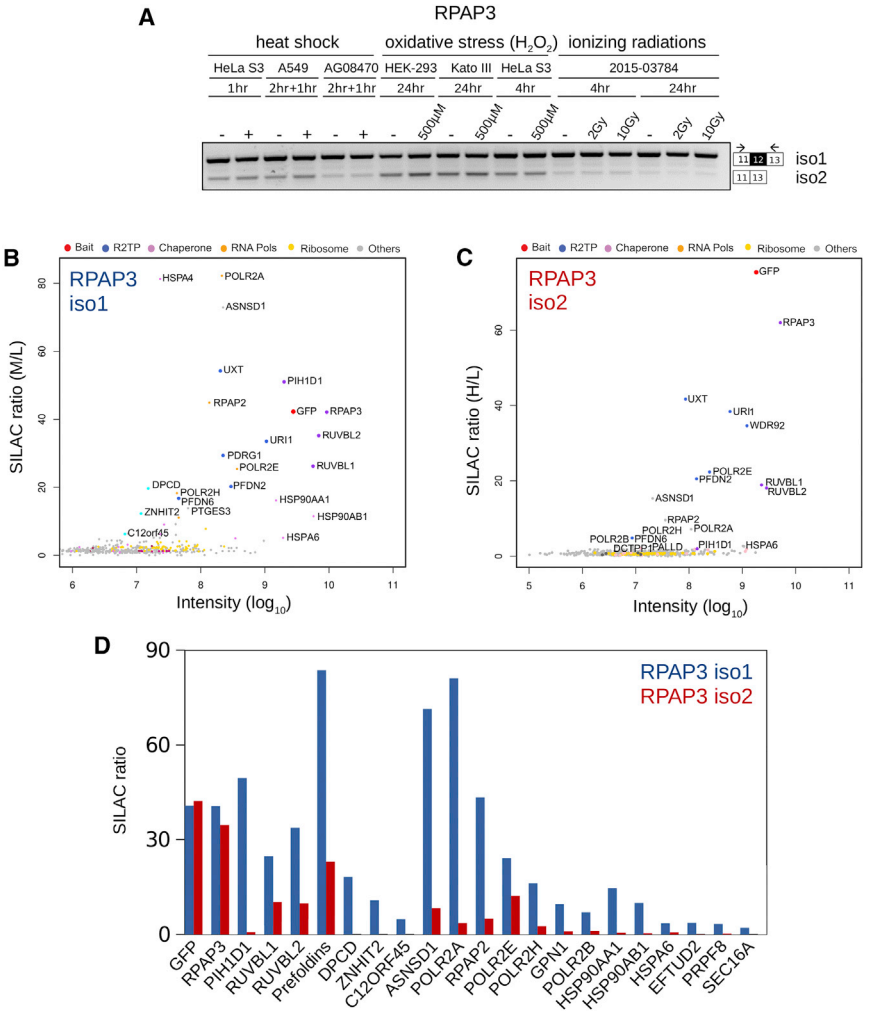

Figure 7. RT-PCR and SILAC IP of RPAP3 Isoforms

(A) Expression of RPAP3 splicing isoforms in different cell types in normal or stress growth conditions. Alternative splicing was evaluated by RT-PCR analysis. The PCR primers amplified RPAP3 transcripts from exon 11 to 13 and are represented by arrowheads on schematized splicing products. HeLa S3, A549, and dermal fibroblast (AG08470) cells were exposed to mild heat shock (42°C for 1 or 2 hr with 1 hr of recovery at 37°C). For oxidative stress, HEK293, Kato-III, and HeLa S3 cells were treated with 500 µM H_2O_2 for 4 or 24 hr. Dermal fibroblasts (2015–03784) were collected 4 or 24 hr after exposure to a single dose of ionizing radiations at 2 or 10 Gy.

(B and C) SILAC proteomic analyses of the RPAP3 interactome, iso1 and iso2 (as in Figure 4B).

(D) Comparison graph showing the SILAC ratios for the most enriched partners found in SILAC IP of RPAP3 iso1 (blue) and iso2 (red). Significance values are listed in Table S1.

DISCUSSION

RPAP3 Regulates HSP90 Activity

The human RPAP3 displays two TPR domains, both exhibiting putative abilities to bind the C-terminal tail of chaperone proteins from the HSP family. We demonstrated the importance of RPAP3-TPR2 and of its helix α7 in the specific recruitment and in the stimulation of HSP90. What is more, our MS data suggest that one dimeric HSP90 could retain up to two molecules of RPAP3. This suggests a model in which RPAP3 interacts with HSP90 through its TPR2 while TPR1 remains free. This possibility is also consistent with our FRET studies, which show that the TPR1+TPR2 fragment has no stabilizing effect on the exchange of HSP90 monomers, as would be expected if TPR1 and TPR2 were to bind simultaneously to the two C-terminal ends of an HSP90 dimer. Our model is thus different from the one proposed previously (Pal et al., 2014), in which a key role in HSP90 binding was assigned to RPAP3 TPR1, with both TPR binding the two ends of an HSP90 dimer. This work was partly based on a fragment of RPAP3 that lacks the segment 382–396, for which a fundamental role in HSP90 binding is described in the present work. When compared, the 3D structures of $RPAP3_{281-396}$ and $RPAP3_{265-381}$ bound to HSP90 displayed high similarity within the TPR domain (Cα RMSD ~ 0.8 Å; Figure S8). However, the peptide enclosed in the X-ray structure (SRMEEVD) is shorter than the one present in our NMR structure (DTSRMEEVD). We have shown that the two first residues D and T promoted important contacts with the root of helix α7. Other structural studies involving TPR domains and HSP peptides also previously highlighted the importance of these elements in the formation of the complex (Blundell et al., 2017). Thus, we believe that our construct possesses supplemental determinants which provide finer information on the interaction between RPAP3 and HSP90.

From this and past studies, we can conclude that the binding of one dimeric HSP90 via the two TPR domains of one RPAP3 could be a too simple way to interpret the interaction. Moreover, our experiments suggest that the N-terminal segment upstream of the tandem TPR, which displays oligomerization features, could stimulate and help stabilize the dimeric form of HSP90. Even in the light of the data obtained in the present study, establishing a realistic model of the interaction mode between RPAP3 and HSP90 remains a challenge. Several hypotheses are possible. First, RPAP3-TPR2 recruits a dimeric HSP90 via the carboxylate-clamp/MEEVD interaction and N-terminal dimerization of RPAP3 would stabilize the complex (Figure 8A). We could imagine a model in which the RPAP3-NTD and/or RPAP3-TPR1 could lean back on the M domain of HSP90, in addition to the strong anchorage provided by the TPR2 (Figure 8B). This model, in which dimerization would also occur via the RPAP3-NTD, has the advantage of locking the HSP90 dimer and of providing TPR1 and NTD of RPAP3 as putative protein regulatory elements. Another possibility is that RPAP3 does not dimerize in presence of HPS90. Under this hypothesis, the HSP90 dimer would be

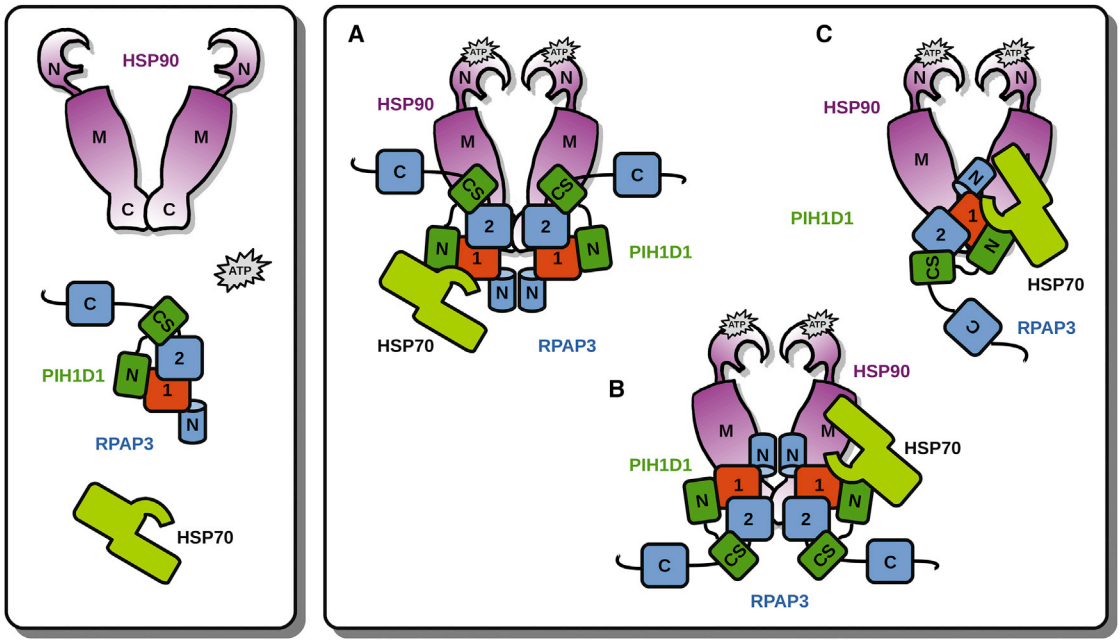

Figure 8. Proposed Models of the Interaction between RPAP3, PIH1D1, HSP70, and HSP90

Dimeric HSP90 is in magenta (N, M, and C designating the N-terminal, middle, and C-terminal sub-domains, respectively), RPAP3 is in orange and blue (N, 1, 2, and C designating the NTD, TPR1, TPR2, and C-terminal domains, respectively), PIH1D1 is in green (N and CS designating the phospho-binding and the CS domains, respectively), HSP70 is in light green and ATP is in gray. (A and B) Two copies of RPAP3 and PIH1D1 are present in alternative positions. (C) One copy of RPAP3 and one copy of PIH1D1 are present.

locked by direct contacts involving the EEVD/RPAP3-TPR2 interaction as well as interactions between TPR1 and/or NTD of RPAP3 and the M domain of HSP90 (Figure 8C).

In all these models, RPAP3-TPR1 would be still available for HSP70 binding since we showed that affinity for the SGPTIEEVD peptide, although weaker than the affinity for HSP90 peptides, was not so negligible (~50 μM). In agreement, SILAC IP showed that, *in vivo*, RPAP3-TPR1 associates with HSP70. Here again, several hypotheses are possible. RPAP3 could act as a bridge for the exchange of protein clients between HSP70 and HSP90. What is more, it provides an opportunity for RPAP3, which is part of the R2TP complex, to address protein client loaded on HSP70 and/or HSP90 to RUVBL proteins. It will be interesting to investigate the number of copies of HSP70 that could be recruited on RPAP3 to evaluate its client loading capacities.

RPAP3:PIH1D1

To study RPAP3 in more detail, we provided data on its interaction with PIH1D1 and showed similarities but also differences with the yeast homologs, Tah1 and Pih1. As observed in the yeast proteins, we demonstrated that $RPAP3_{396-445}$ folded upon PIH1D1 CS domain binding, until it formed intermolecular β sheets (Figure S8). Poor sequence conservation in the Pih1/PIH1D1 binding sites of Tah1 and RPAP3 was not a barrier to achieve similar secondary structures that involve backbone of the proteins. In yeast, X-ray and NMR analysis of the Tah1:Pih1 complex revealed differences in the relative orientation of the two partners, suggesting potential plasticity of the complex (Quinternet et al., 2015). However, for yeast proteins, we noted a structural feature that was common to the NMR and X-ray studies. The 10 last residues (from position 101 to 111) in the tail of Tah1, and located downstream of the β strands, formed a protective loop for hydrophobic residues, all located on the β1-β2-β6-β7 face of the Pih1 CS domain (Figure S8). In the human complex, this protective role toward the same corresponding face in PIH1D1 is endorsed by residues in RPAP3 located upstream of the β strands 1 and 2, more precisely in helices α7 and α8, as well as in the region 409–431 (Figures 6 and S8). Interestingly, we demonstrated that this long embracing segment included the supplemental 34-residue segment only found in RPAP3 iso1. As a result, the orientation of PIH1D1 toward RPAP3 is very constrained and totally differs from the one observed with the yeast proteins (Figure S8). Consequently, relative motions of the two human proteins are less likely than for the yeast complex. Thus, if we refer to our models of interaction between RPAP3 and HSP90, this indicates that PIH1D1 could be found close to HSP90 (Figure 8). By the way, RPAP3, which regulates HSP90 alone, could bring an additional potential protein regulator to finely modulate the ATPase activity of the chaperone. Unfortunately, ATPase activity tests performed on HSP90 using PIH1D1 and RPAP3 simultaneously led to data that were tricky to analyze clearly (data not shown). Furthermore, via its N-terminal domain, PIH1D1 is able to bind phosphorylated substrates (Horejsi et al., 2014). The locking of the CS domain of PIH1D1 into RPAP3 as well as secondary contacts between PIH1D1-N and RPAP3-TPR1 could trigger the correct positioning of the phosphorylated clients for their right addressing to or by the chaperones.

The tight binding observed between RPAP3 iso1 and PIH1D1 reminds the one observed between snoRNP assembly factors

Rsa1/NUFIP1 and Hit1/ZNHIT3 (Quinternet et al., 2016). The latter have even be considered as a unique protein. We could extend this consideration to human RPAP3 and PIH1D1 proteins. Interestingly, we demonstrated that both iso1 and iso2 of RPAP3 mRNA could co-exist in different cell lines. However, iso2 could not strongly bind PIH1D1. Thus, the cell leaves the possibility to RPAP3 to work differently. Being free of PIH1D1, RPAP3 iso2 would create a R2T complex containing RUVBL proteins and still able to bind HSP90 and HSP70. SILAC proteomics indicate that this complex exists and that its partners are both distinct and similar than R2TP. This could set up a competition between the R2TP and the R2T in the cell. Finally, we aimed at investigating the factors that could regulate alternative splicing of RPAP3 using semi-qRT-PCR. Interestingly, we were not able to highlight external factors such as stresses that could unbalance the equilibrium between the two isoforms of RPAP3. It suggests that R2TP and R2T complexes could be constitutive in the cell and that they both have a role to play.

STAR★METHODS

Detailed methods are provided in the online version of this paper and include the following:

- KEY RESOURCES TABLE
- CONTACT FOR REAGENT AND RESOURCE SHARING
- EXPERIMENTAL MODEL AND SUBJECT DETAILS
  - Culture Conditions
- METHOD DETAILS
  - Purification of Isolated TPR Domains and TPR Tandem of Human RPAP3 for NMR and MS Analysis
  - Peptides Preparation
  - Chemical Shift Mapping and Kd Measurement Using NMR
  - NMR Structure Calculations
  - NMR Binding Assays between the N-Terminal Domain of PIH1D1 and TPR Domains of RPAP3
  - Yeast 2-Hybrid Assays
  - Non Denaturing Mass Spectrometry
  - IP-LUMIER Assays
  - Plasmids Used for Studying the HSP90 Chaperone Cycle
  - Expression Strains Used for Studying the HSP90 Chaperone Cycle
  - Proteins Used for Studying the HSP90 Chaperone Cycle
  - Analytical Size-Exclusion Chromatography
  - Kinetic ATPase Assay
  - Dimer Subunits Exchange
  - Cell Culture and RT-PCR
  - SILAC-IP and Proteomic Analysis
  - Protein Coexpression Assays
  - Purification of the $RPAP3_{281-445}$:$PIH1D1_{199-290}$ Complex
  - Crystallization, Data Collection and Structure Determination of the $RPAP3_{281-445}$:$PIH1D1_{199-290}$ Complex
- QUANTIFICATION AND STASTISTICAL ANALYSIS
- DATA AND SOFTWARE AVAILABILITY

SUPPLEMENTAL INFORMATION

Supplemental Information includes eight figures and two tables and can be found with this article online at https://doi.org/10.1016/j.str.2018.06.002.

ACKNOWLEDGMENTS

This work was supported by the CNRS, University of Lorraine, University of Strasbourg, the Région Grand Est, the Agence Nationale de la Recherche [ANR-11-BSV8-01503; ANR-16-CE11-0032-02], the PRST IMTS of Plan Etat Région Lorraine and the French Proteomic Infrastructure (ProFI; ANR-10-INBS-08-03). We thank UMS 2008 for ITC and NMR facilities. G.T. and M.B. acknowledges the Région Alsace and Novalix for supporting their PhD fellowships. We thank the ESRF beamline ID30-A and SOLEIL beamlines Proxima-1 and -2 for X-ray diffraction facility. We thank GIS IBiSA and Région Alsace for financial support in purchasing a Synapt G2 HDMS instrument. Mass spectrometry analysis of SILAC IP experiments were performed on the Functional Proteomics Platform in Montpellier, France. F.G. and P.M. acknowledge Sorbonne Université, the support of the Foundation ARC and the ITMO cancer of Plan Cancer 2014–2019. P.M. also acknowledges the help of Hélène Bret.

AUTHOR CONTRIBUTIONS

Conceptualization, M.Q., J.H., M.-E.C., P.M., E.B., S.C., and X.M.; Validation, all co-authors; Investigation, all co-authors; Writing – Original Draft, M.Q., J.H., S.C., and X.M.; Writing – Review & Editing, all co-authors; Visualization, M.Q., J.H., C.A., M.B., G.T., Y.A., and C.V.; Supervision, M.Q., J.H., I.B.-A., P.M., E.B., S.C., and X.M.; Funding Acquisition, P.M., B.C., S.C., X.M., and E.B.

DECLARATION OF INTERESTS

The authors declare no competing interests.

Received: March 15, 2018
Revised: May 4, 2018
Accepted: June 8, 2018
Published: July 19, 2018

REFERENCES

Adams, P.D., Afonine, P.V., Bunkoczi, G., Chen, V.B., Davis, I.W., Echols, N., Headd, J.J., Hung, L.W., Kapral, G.J., Grosse-Kunstleve, R.W., et al. (2010). PHENIX: a comprehensive Python-based system for macromolecular structure solution. Acta Crystallogr. D Biol. Crystallogr. *66*, 213–221.

Afonine, P.V., Grosse-Kunstleve, R.W., Echols, N., Headd, J.J., Moriarty, N.W., Mustyakimov, M., Terwilliger, T.C., Urzhumtsev, A., Zwart, P.H., and Adams, P.D. (2012). Towards automated crystallographic structure refinement with phenix.refine. Acta Crystallogr. D Biol. Crystallogr. *68*, 352–367.

Anthis, N.J., and Clore, G.M. (2013). Sequence-specific determination of protein and peptide concentrations by absorbance at 205 nm. Protein Sci. *22*, 851–858.

Back, R., Dominguez, C., Rothe, B., Bobo, C., Beaufils, C., Morera, S., Meyer, P., Charpentier, B., Branlant, C., Allain, F.H., et al. (2013). High-resolution structural analysis shows how Tah1 tethers Hsp90 to the R2TP complex. Structure *21*, 1834–1847.

Benbahouche Nel, H., Iliopoulos, I., Torok, I., Marhold, J., Henri, J., Kajava, A.V., Farkas, R., Kempf, T., Schnolzer, M., Meyer, P., et al. (2014). Drosophila Spag is the homolog of RNA polymerase II-associated protein 3 (RPAP3) and recruits the heat shock proteins 70 and 90 (Hsp70 and Hsp90) during the assembly of cellular machineries. J. Biol. Chem. *289*, 6236–6247.

Bertini, I., Luchinat, C., Parigi, G., Ravera, E., Reif, B., and Turano, P. (2011). Solid-state NMR of proteins sedimented by ultracentrifugation. Proc. Natl. Acad. Sci. USA *108*, 10396–10399.

Blundell, K.L., Pal, M., Roe, S.M., Pearl, L.H., and Prodromou, C. (2017). The structure of FKBP38 in complex with the MEEVD tetratricopeptide binding-motif of Hsp90. PLoS One *12*, e0173543.

Boulon, S., Marmier-Gourrier, N., Pradet-Balade, B., Wurth, L., Verheggen, C., Jady, B.E., Rothe, B., Pescia, C., Robert, M.C., Kiss, T., et al. (2008). The Hsp90 chaperone controls the biogenesis of L7Ae RNPs through conserved machinery. J. Cell Biol. *180*, 579–595.

Boulon, S., Pradet-Balade, B., Verheggen, C., Molle, D., Boireau, S., Georgieva, M., Azzag, K., Robert, M.C., Ahmad, Y., Neel, H., et al. (2010). HSP90 and its R2TP/Prefoldin-like cochaperone are involved in the cytoplasmic assembly of RNA polymerase II. Mol. Cell *39*, 912–924.

Chagot, M.E., Jacquemin, C., Branlant, C., Charpentier, B., Manival, X., and Quinternet, M. (2015). (1)H, (15)N and (13)C resonance assignments of the two TPR domains from the human RPAP3 protein. Biomol. NMR Assign. *9*, 99–102.

Eckert, K., Saliou, J.M., Monlezun, L., Vigouroux, A., Atmane, N., Caillat, C., Quevillon-Cheruel, S., Madiona, K., Nicaise, M., Lazereg, S., et al. (2010). The Pih1-Tah1 cochaperone complex inhibits Hsp90 molecular chaperone ATPase activity. J. Biol. Chem. *285*, 31304–31312.

Emsley, P., and Cowtan, K. (2004). Coot: model-building tools for molecular graphics. Acta Crystallogr. D Biol. Crystallogr. *60*, 2126–2132.

Horejsi, Z., Stach, L., Flower, T.G., Joshi, D., Flynn, H., Skehel, J.M., O'Reilly, N.J., Ogrodowicz, R.W., Smerdon, S.J., and Boulton, S.J. (2014). Phosphorylation-dependent PIH1D1 interactions define substrate specificity of the R2TP cochaperone complex. Cell Rep. *7*, 19–26.

Houry, W.A., Bertrand, E., and Coulombe, B. (2018). The PAQosome, an R2TP-based chaperone for quaternary structure formation. Trends Biochem. Sci. *43*, 4–9.

Jackson, S.E. (2013). Hsp90: structure and function. Top. Curr. Chem. *328*, 155–240.

Jecklin, M.C., Touboul, D., Bovet, C., Wortmann, A., and Zenobi, R. (2008). Which electrospray-based ionization method best reflects protein-ligand interactions found in solution? A comparison of ESI, nanoESI, and ESSI for the determination of dissociation constants with mass spectrometry. J. Am. Soc. Mass Spectrom. *19*, 332–343.

Lalevee, S., Bour, G., Quinternet, M., Samarut, E., Kessler, P., Vitorino, M., Bruck, N., Delsuc, M.A., Vonesch, J.L., Kieffer, B., et al. (2010). Vinexinss, an atypical "sensor" of retinoic acid receptor gamma signaling: union and sequestration, separation, and phosphorylation. FASEB J. *24*, 4523–4534.

Li, J., Richter, K., and Buchner, J. (2011). Mixed Hsp90-cochaperone complexes are important for the progression of the reaction cycle. Nat. Struct. Mol. Biol. *18*, 61–66.

Lopez-Mendez, B., and Guntert, P. (2006). Automated protein structure determination from NMR spectra. J. Am. Chem. Soc. *128*, 13112–13122.

Martino, F., Pal, M., Munoz-Hernandez, H., Rodriguez, C.F., Nunez-Ramirez, R., Gil-Carton, D., Degliesposti, G., Skehel, J.M., Roe, S.M., Prodromou, C., et al. (2018). RPAP3 provides a flexible scaffold for coupling HSP90 to the human R2TP co-chaperone complex. Nat. Commun. *9*, 1501.

Maurizy, C., Quinternet, M., Abel, Y., Verheggen, C., Santo, P.E., Bourguet, M., Paiva, A.C.F., Bragantini, B., Chagot, M.-E., Robert, M.-C., et al. (2018). The RPAP3-Cterminal domain identifies R2TP-like quaternary chaperones. Nat. Commun. https://doi.org/10.1038/s41467-018-04431-1.

Meyer, P., Prodromou, C., Hu, B., Vaughan, C., Roe, S.M., Panaretou, B., Piper, P.W., and Pearl, L.H. (2003). Structural and functional analysis of the middle segment of hsp90: implications for ATP hydrolysis and client protein and cochaperone interactions. Mol. Cell *11*, 647–658.

Meyer, P., Prodromou, C., Liao, C., Hu, B., Roe, S.M., Vaughan, C.K., Vlasic, I., Panaretou, B., Piper, P.W., and Pearl, L.H. (2004). Structural basis for recruitment of the ATPase activator Aha1 to the Hsp90 chaperone machinery. EMBO J. *23*, 1402–1410.

Pal, M., Morgan, M., Phelps, S.E., Roe, S.M., Parry-Morris, S., Downs, J.A., Polier, S., Pearl, L.H., and Prodromou, C. (2014). Structural basis for phosphorylation-dependent recruitment of Tel2 to Hsp90 by Pih1. Structure *6*, 805–818.

Panaretou, B., Sinclair, K., Prodromou, C., Johal, J., Pearl, L., and Piper, P.W. (1999). The Hsp90 of *Candida albicans* can confer Hsp90 functions in *Saccharomyces cerevisiae*: a potential model for the processes that generate immunogenic fragments of this molecular chaperone in *C. albicans* infections. Microbiology *145* (Pt 12), 3455–3463.

Prodromou, C., Siligardi, G., O'Brien, R., Woolfson, D.N., Regan, L., Panaretou, B., Ladbury, J.E., Piper, P.W., and Pearl, L.H. (1999). Regulation of Hsp90 ATPase activity by tetratricopeptide repeat (TPR)-domain co-chaperones. EMBO J. *18*, 754–762.

Quinternet, M., Chagot, M.E., Rothe, B., Tiotiu, D., Charpentier, B., and Manival, X. (2016). Structural features of the box C/D snoRNP pre-assembly process are conserved through species. Structure *24*, 1693–1706.

Quinternet, M., Rothe, B., Barbier, M., Bobo, C., Saliou, J.M., Jacquemin, C., Back, R., Chagot, M.E., Cianferani, S., Meyer, P., et al. (2015). Structure/function analysis of protein-protein interactions developed by the yeast Pih1 platform protein and its partners in box C/D snoRNP assembly. J. Mol. Biol. *427*, 2816–2839.

Retzlaff, M., Hagn, F., Mitschke, L., Hessling, M., Gugel, F., Kessler, H., Richter, K., and Buchner, J. (2010). Asymmetric activation of the Hsp90 dimer by its cochaperone Aha1. Mol. Cell *37*, 344–354.

Rivera-Calzada, A., Pal, M., Munoz-Hernandez, H., Luque-Ortega, J.R., Gil-Carton, D., Degliesposti, G., Skehel, J.M., Prodromou, C., Pearl, L.H., and Llorca, O. (2017). The structure of the R2TP complex defines a platform for recruiting diverse client proteins to the HSP90 molecular chaperone system. Structure *25*, 1145–1152.e4.

Shen, Y., Delaglio, F., Cornilescu, G., and Bax, A. (2009). TALOS+: a hybrid method for predicting protein backbone torsion angles from NMR chemical shifts. J. Biomol. NMR *44*, 213–223.

Shiau, A.K., Harris, S.F., Southworth, D.R., and Agard, D.A. (2006). Structural analysis of *E. coli* hsp90 reveals dramatic nucleotide-dependent conformational rearrangements. Cell *127*, 329–340.

Siligardi, G., Hu, B., Panaretou, B., Piper, P.W., Pearl, L.H., and Prodromou, C. (2004). Co-chaperone regulation of conformational switching in the Hsp90 ATPase cycle. J. Biol. Chem. *279*, 51989–51998.

Tian, S., Yu, G., He, H., Zhao, Y., Liu, P., Marshall, A.G., Demeler, B., Stagg, S.M., and Li, H. (2017). Pih1p-Tah1p puts a lid on hexameric AAA+ ATPases Rvb1/2p. Structure *25*, 1519–1529.e4.

Tosi, A., Haas, C., Herzog, F., Gilmozzi, A., Berninghausen, O., Ungewickell, C., Gerhold, C.B., Lakomek, K., Aebersold, R., Beckmann, R., et al. (2013). Structure and subunit topology of the INO80 chromatin remodeler and its nucleosome complex. Cell *154*, 1207–1219.

Yoshida, M., Saeki, M., Egusa, H., Irie, Y., Kamano, Y., Uraguchi, S., Sotozono, M., Niwa, H., and Kamisaki, Y. (2013). RPAP3 splicing variant isoform 1 interacts with PIH1D1 to compose R2TP complex for cell survival. Biochem. Biophys. Res. Commun. *430*, 320–324.

Zhao, R., and Houry, W.A. (2005). Hsp90: a chaperone for protein folding and gene regulation. Biochem. Cell Biol. *83*, 703–710.

Zhao, R., Kakihara, Y., Gribun, A., Huen, J., Yang, G., Khanna, M., Costanzo, M., Brost, R.L., Boone, C., Hughes, T.R., et al. (2008). Molecular chaperone Hsp90 stabilizes Pih1/Nop17 to maintain R2TP complex activity that regulates snoRNA accumulation. J. Cell Biol. *180*, 563–578.

STAR★METHODS

KEY RESOURCES TABLE

REAGENT or RESOURCE	SOURCE	IDENTIFIER
Antibodies		
M2 antibodies for Lumier-IP	Sigma	Cat#F1804; RRID:AB_262044
IP GFP TrapA for SILAC-IP	Chromotek	Cat#Gta-100; RRID:AB_2631357
Bacterial and Virus Strains		
E. coli (BL21) pRARE 2	Lab strain	N/A
Rosetta2(DE3)	Merck-Millipore	Cat#71400
Chemicals, Peptides, and Recombinant Proteins		
Peptide: MEEVD	GeneCust, Proteogenix	http://www.genecust.com/fr/ https://www.proteogenix.science/
Peptide: DTSRMEEVD	GeneCust, Proteogenix	http://www.genecust.com/fr/ https://www.proteogenix.science/
Peptide: DASRMEEVD	GeneCust, Proteogenix	http://www.genecust.com/fr/ https://www.proteogenix.science/
Peptide: SGPTIEEVD	GeneCust, Proteogenix	http://www.genecust.com/fr/ https://www.proteogenix.science/
Protein: $RPAP3_{133-255}$ (RPAP3-TPR1)	{Chagot et al., 2015 #5065}	N/A
Protein: $RPAP3_{281-396}$ (RPAP3-TPR2)	{Chagot et al., 2015 #5065}	N/A
Protein: $RPAP3_{281-445}$	This study	N/A
Protein: $RPAP3_{396-430}$	This study	N/A
Protein: $RPAP3_{396-455}$	This study	N/A
Protein: $RPAP3_{281-455\Delta iso}$	This study	N/A
Protein: $RPAP3_{281-455}$	This study	N/A
Protein: $RPAP3_{133-396}$ (tandem)	This study	N/A
Protein: $PIH1D1_{1-290}$	This study	N/A
Protein: $PIH1D1_{1-180}$ (PIH1D1-N)	This study	N/A
Protein: $PIH1D1_{181-290}$	This study	N/A
Protein: $PIH1D1_{199-290}$ (PIH1D1-CS)	This study	N/A
Protein: $PIH1D1_{209-290}$	This study	N/A
Cesium iodide, 99.9%, for analysis, ACROS Organics™	Fisher Scientific	Cat#10554131
Myoglobin from equine heart ≥90% (SDS-PAGE), essentially salt-free, lyophilized powder	Sigma Aldrich	Cat#M1882
Ammonium acetate for molecular biology, ≥98%	Sigma Aldrich	Cat#A1542
Isopropanol, for HPLC	Fisher Scientific	Cat#10674732
Formic acid, reagent grade, ≥95%	Sigma Aldrich	Cat#F0507
Acetonitrile, for HPLC	Fisher Scientific	Cat#10407440
GLUCOSE-D U-13C6 99%13C	Eurisotop	Cat#CLM-1396-10
AMMONIUM CHLORIDE 15N 98%+15N	Eurisotop	Cat# NLM-467-5
DEUTERIUM OXIDE 99.97%D	Eurisotop	Cat# D215T
3-amino-1,2,4-triazol	Sigma	Cat#A8056
Homo sapiens RPAP3 recombinant proteins	This study	Hs-RPAP3
Homo sapiens HSP90 recombinant proteins	This study	Hs-HSP90
Saccharomyces cerevisiae Hsp82 recombinant protein	This study	Sc-Hsp90
Saccharomyces cerevisiae Aha1 truncation 1-153 recombinant protein	This study	Sc-Aha1(1-153)

(*Continued on next page*)

Continued

REAGENT or RESOURCE	SOURCE	IDENTIFIER
Critical Commercial Assays		
Lumier assay with dual luciferase kit	Promega	Cat#DLAK-01
Gateway system for cloning orf for Y2H and lumier and SILAC assay	Thermo Fisher Scientific	N/A
Deposited Data		
Chemical Shifts of $RPAP3_{133-255}$	{Chagot et al., 2015 #5065}	PDB: 6FD7
NMR Structure of $RPAP3_{133-255}$	This study	PDB: 6FD7
Chemical Shifts of $RPAP3_{281-396}$:DTSRMEEVD	This study	BMRB: 34223
NMR structure of $RPAP3_{281-396}$:DTSRMEEVD	This study	PDB: 6FDP
Chemical Shifts of $RPAP3_{281-396}$:SGPTIEEVD	This study	BMRB: 34224
NMR structure of $RPAP3_{281-396}$:SGPTIEEVD	This study	PDB: 6FDT
Crystal structure of $RPAP3_{281-445}$:$PIH1D1_{199-290}$	This study	PDB: 6GXZ
Experimental Models: Cell Lines		
A549	ECACC	Cat#86012804
Kato-III	ECACC	Cat#86093004
Dermal healthy fibroblasts	Coriell Cell Repositories	Cat#AG08470
Dermal healthy fibroblasts	Institut de Cancérologie de Lorraine (ICL, Nancy)	2015-03784
Hek-293	Institut de Génétique et de Biologie Moléculaire (IGBMC, Strasbourg)	N/A
HeLa S3	Institut de Génétique et de Biologie Moléculaire (IGBMC, Strasbourg)	N/A
Experimental Models: Organisms/Strains		
Hela Flip-in cells expressing GFP-PAP3 isoform 1	Institut de Génétique Moléculaire de Montpellier	N/A
Hela Flip-in cells expressing GFP-PAP3 isoform 2	Institut de Génétique Moléculaire de Montpellier	N/A
Hela Flip-in cells expressing GFP-PAP3 TPR1	Institut de Génétique Moléculaire de Montpellier	N/A
HEK 293 T for lumier assay	Institut de Génétique Moléculaire de Montpellier	N/A
Saccharomyces cerevisiae strain CG1945 for Y2H	Institut de Génétique Moléculaire de Montpellier	N/A
Saccharomyces cerevisiae strain Y187 for Y2H	Institut de Génétique Moléculaire de Montpellier	N/A
Oligonucleotides		
See Table S2		
Recombinant DNA		
$RPAP3_{133-255}$ (RPAP3-TPR1) in pnEA-3CH and pnYK vectors	{Chagot et al., 2015 #5065}	N/A
$RPAP3_{281-396}$ (RPAP3-TPR2) in pnEA-3CH and pnYK vectors	{Chagot et al., 2015 #5065}	N/A
$RPAP3_{281-445}$ in pnEA-3CH and pnYK vectors	This study	N/A
$RPAP3_{396-430}$ in pnEA-3CH and pnYK vectors	This study	N/A
$RPAP3_{396-455}$ in pnEA-3CH and pnYK vectors	This study	N/A
$RPAP3_{281-455\Delta iso}$ in pnEA-3CH and pnYK vectors	This study	N/A
$RPAP3_{281-455}$ in pnEA-3CH and pnYK vectors	This study	N/A
$RPAP3_{133-396}$ (tandem) in pnEA-3CH and pnYK vectors	This study	N/A
$PIH1D1_{1-290}$ in pnEA-3CH and pnYK vectors	This study	N/A
$PIH1D1_{181-290}$ in pnEA-3CH and pnYK vectors	This study	N/A

(*Continued on next page*)

Continued

REAGENT or RESOURCE	SOURCE	IDENTIFIER
PIH1D1$_{199-290}$ in pnEA-3CH and pnYK vectors	This study	N/A
PIH1D1$_{209-290}$ in pnEA-3CH and pnYK vectors	This study	N/A
RPAP3(FL) in pnEA-3CH and pnYK vectors	This study	N/A
His6-RPAP3(133-396) expression plasmid	This study	N/A
His6-RPAP3(1-396) expression plasmid	This study	N/A
Software and Algorithms		
CYANA 3.97	{Lopez-Mendez and Guntert, 2006 #3848}	http://www.cyana.org/
TALOS+	{Shen et al., 2009 #3859}	https://spin.niddk.nih.gov/bax/software/TALOS/
AMBER	{Bertini et al., 2011 #3987}	http://py-enmr.cerm.unifi.it
PHENIX.REFINE	{Afonine et al., 2012 #5166}	https://www.phenix-online.org/
PHENIX Suite	{Adams et al., 2010 #5235}	https://www.phenix-online.org/
MassLynx V4.1	Waters	http://www.waters.com/waters/fr_FR/MassLynx-MS-Software/nav.htm?locale=fr_FR&cid=513662
COOT	{Emsley and Cowtan, 2004 #5209}	http://www2.mrc-lmb.cam.ac.uk/personal/pemsley/coot

CONTACT FOR REAGENT AND RESOURCE SHARING

Further information and requests for resources and reagents should be directed to, and will be fulfilled by, the lead contact, Marc Quinternet (marc.quinternet@univ-lorraine.fr).

EXPERIMENTAL MODEL AND SUBJECT DETAILS

Culture Conditions

E. coli BL21(DE3) pRARE2 were grown in selective solid and liquid LB medium or liquid M9 medium at 20° or 37°C degrees. *E. coli* BL21(DE3) Rosetta2-pLysSRAR were grown in selective solid LB medium or liquid 2xYT medium at 30° or 37°C. *Saccharomyces cerevisiae* strains (CG1945 and Y187) were grown on selective or non-selective YEPD at 30°C. A549, HeLa S3, HeLa H9, HEK-293, HEK-293T and dermal fibroblast cells were cultured in Dulbecco's modified Eagle medium (DMEM) and Kato-III in RPMI medium 1640. Dermal fibroblasts, Hela S3, Hela-H9, HEK-293 and HEK-293T were female cell lines. A549 and Kato-III were male cell lines. More details on growth conditions are found in the Method Details section.

METHOD DETAILS

Purification of Isolated TPR Domains and TPR Tandem of Human RPAP3 for NMR and MS Analysis

Overexpression, purification and sample conditions of soluble $^{13}C/^{15}N$-labelled RPAP3$_{133-255}$ and RPAP3$_{281-396}$ domains have been previously described in details (Chagot et al., 2015). RPAP3$_{133-396}$ and RPAP3$_{281-445}$ were prepared using the same protocol starting from pnEA-3CH vectors enclosing the DNA sequence of regions 133-396 and 281-445 in RPAP3. Briefly, his-tagged version of the protein domains were overexpressed in a *E. coli* BL21(DE3) pRARE2 strain at 20°C in a minimal M9 medium supplemented with $^{15}NH_4Cl$ and ^{13}C-d6-glucose for NMR samples and non-labelled sodium and carbon sources for ITC and MS samples. Affinity chromatography steps performed on TALON beads permitted to isolate the recombinant his-tagged proteins from the whole cellular lysate. Elution from the beads was performed using the 3C prescission protease. A final size-exclusion chromatography in 10 mM NaPi (pH 6.4), 150 mM NaCl, 0.5 mM TCEP (NMR buffer) permitted to recover pure protein fractions. The purification was followed on denaturing 12.5% SDS-Polyacrylamide gels. Fractions corresponding to the desired proteins were pooled and concentration was assessed using molar extinction coefficient at 280 nm.

Peptides Preparation

The following peptides (GeneCust, Luxemburg and Proteogenix, France) have been used in this study: DTSRMEEVD (HSP90α), DASRMEEVD (HSP90β), MEEVD and SGPTIEEVD (HSP70). Peptides were accurately weighted then dissolved in water. Precise concentration was successfully calculated using molar extinction coefficient at 205 nm since any of the sequences display Tyr and/or Trp residues (Anthis and Clore, 2013). Solutions were then lyophilized, suspended in Phosphate buffer 10 mM, pH 6.4, NaCl 150 mM and pH was adjusted using 0.5 M NaOH.

Chemical Shift Mapping and Kd Measurement Using NMR

Series of ^{1}H-^{15}N HSQC spectra were recorded on $^{13}C/^{15}N$-labelled $RPAP3_{133-255}$, $RPAP3_{281-396}$ or $RPAP3_{133-396}$ with increasing amounts of peptide DTSRMEEVD, DASRMEEVD, MEEVD or SGPTIEEVD. The chemical shift perturbation for backbone amide groups was evaluated through a composite value calculated as follow: $\Delta\delta = \sqrt{0.1(\delta^{15}N)^2 + (\delta^{1}H)^2}$. Data were used (i), to map the peptide binding site on proteins and (ii), to assess the dissociation constant Kd using an in-house python script as already described (Lalevee et al., 2010). Protein concentrations were around 100 μM in 10 mM NaPi (pH 6.4), 150 mM NaCl, 0.5 mM TCEP, 5% D_2O. Data were collected at 293 K on a 600 MHz spectrometer equipped with a TCI-cryoprobe (Bruker).

NMR Structure Calculations

All NMR experiments needed for solution structure determination were performed on a 600 MHz spectrometer equipped with a cryoprobe (Bruker), at 293K for $RPAP3_{281-396}$:HSP90α and $RPAP3_{281-396}$:HSP70 complexes, and at 303K for the free $RPAP3_{133-255}$. For the $RPAP3_{281-396}$:HSP90α and $RPAP3_{281-396}$:HSP70 complexes, a 1:1 sample containing $^{13}C/^{15}N$-labelled protein and unlabelled synthetic peptide was prepared with a final concentration of 1 mM in Phosphate buffer 10 mM, pH 6.4, NaCl 150 mM, 0.5 mM TCEP, 5% D_2O. For the free $RPAP3_{133-255}$ domain, the almost complete resonance assignment was previously described (BMRB entry 19758) (Chagot et al., 2015). For $RPAP3_{281-396}$:HSP90α and $RPAP3_{281-396}$:HSP70, the almost complete resonance assignment of bound forms of $RPAP3_{281-396}$ was achieved using a classical approach based on 3D NMR spectra with help of the free form assignment (BMRB entry 19757) (Chagot et al., 2015). For the bound forms of HSP90α and HSP70 peptides, the resonance assignment was performed using double X half-filter NOESY and TOCSY spectra. Chemical shifts data referenced to DSS were deposited in the Biological Magnetic Resonance Data Bank under entry 34223 and 34224 for $RPAP3_{281-396}$:DTSRMEEVD and $RPAP3_{281-396}$:SGPTIEEVD respectively. For structure determination, distances were derived from NOESY-HSQC ^{1}H-^{15}N and ^{1}H-^{13}C NMR experiments. Interchain distances were derived from 3D X half-filter ^{1}H-^{13}C-HSQC-NOESY, 3D X half-filter ^{1}H-^{15}N NOESY-HSQC and 2D X half-filter ^{1}H-^{1}H NOESY spectra recorded in H_2O and D_2O. Intra-peptide distances were derived from double X half-filter recorded in H_2O and D_2O. Dihedral restraints were derived from TALOS+ (Shen et al., 2009). The NMR structures of $RPAP3_{133-255}$, $RPAP3_{281-396}$:HSP90α and $RPAP3_{281-396}$:HSP70 were calculated using the automated procedure of CYANA 3.0 (Lopez-Mendez and Guntert, 2006). NOE assignments were carefully checked after the final iteration. For each object, 200 structures calculated with the final set of restraints provided by CYANA 3.0 and TALOS+ were refined in explicit water using the AMBER-based Portal Server for NMR structures (AMPS-NMR) (Bertini et al., 2011). Finally, the 20 structures with the lowest restraint energies were selected as the most representative structures and were deposited in the Protein Data Bank under reference 6FD7, 6FDP and 6FDT, for $RPAP3_{133-255}$, $RPAP3_{281-396}$:HSP90α and $RPAP3_{281-396}$:HSP70 respectively.

NMR Binding Assays between the N-Terminal Domain of PIH1D1 and TPR Domains of RPAP3

Fragment 1-180 of human PIH1D1 (PIH1D1-N) was cloned into a pnEA-3CH vector and purified as described above for non-labelled isolated TPR domains of RPAP3. The final sample was placed into the NMR buffer described above. ^{1}H-^{15}N HSQC spectra of ^{15}N-labelled samples of $RPAP3_{133-255}$, $RPAP3_{133-396}$ and $RPAP3_{281-396}$ were recorded at 600 MHz, 293 K in absence or in presence of a 3-fold excess of $PIH1D1_{1-180}$. The protein concentration of ^{15}N labelled samples was around 50 μM.

Yeast 2-Hybrid Assays

Plasmids pACT2 and pAS2 were introduced into haploid *Saccharomyces cerevisiae* strains (CG1945 and Y187, respectively). Strains were crossed on yeast extract peptone dextrose (YEPD) complete media overnight. The day after diploids were plated on −Leu −Trp control growth media and on triple selective media (−Leu −Trp −His). Growth was assessed visually after three days of incubation at 30°C. The strength of interactions was evaluated by comparing the number of clones growing on −Leu −Trp (selection of diploids) and −Leu −Trp −His plates (selection for interaction). 10 mM of 3-amino-1,2,4-triazol (3AT) (Sigma) was used to evaluate the strength of the interaction.

Non Denaturing Mass Spectrometry

For native MS experiments, proteins were buffer exchanged against 150 mM (HSP:RPAP3 samples) or 300 mM (PIH1D1:RPAP3 complexes) ammonium acetate buffer (from Sigma, St. Louis, MO, USA), pH 7.5 or 6.9, respectively, using Zeba microcentrifuge gel filtration columns (2 cycles) (from Thermo Fisher Scientific, Rockford, IL, USA). Protein concentrations were determined by UV absorbance using a NanoDrop 2000 spectrophotometer (Thermo Fisher Scientific, France).

Mass spectrometry experiments were carried out on an electrospray time-of-flight mass spectrometer (LCT, Waters, Manchester, UK), or on an hybrid electrospray quadrupole time-of-flight mass spectrometer (Synapt G2 HDMS, Waters, Manchester, UK) equipped with an automated chip-based nanoelectrospray source (Triversa Nanomate, Advion Biosciences, Ithaca, U.S.A.) operating in the positive ion mode. Denatured MS analysis was performed with external calibration using the multiply charged ions produced by 2 μM horse heart myoglobin solution diluted in water/acetonitrile/formic acid (50v/50v/1v) and classical interface tuning parameters of the mass spectrometer (Vc, 40 V; Pi, 2.1 mbar). For native MS experiments, external calibration was performed using singly charged ions produced by a 2 mg/mL solution of cesium iodide in 2-propanol/water (1v/1v). Instrumental parameters were carefully optimized to improve desolvation and ion transfer as well as maintaining non covalent interactions. These optimizations are

particularly related to the pressure (Pi) during the first pumping stage, and the sample cone voltage (Vc) (see below). Native MS data interpretation was performed using MassLynx 4.1 (Waters, Manchester, UK).

To determine dissociation constants, individuals TPR (20 μM) were incubated with increasing peptide concentrations (0, 4, 20, 75 and 100 μM). For each analysis, the peak intensity of free protein (I_P) and protein/peptide complex (I_{PL}) was recorded for charge states referring to native protein or complex (i.e. 6+ and 7+). From the establishment of a graph representing the intensity I_{PL} as a function of ligand concentration, a mathematical model can be adjusted (Jecklin et al., 2008), and the K_d values determined.

To determine relative affinity of tandem $RPAP3_{133-396}$ for peptides, the tandem (20 μM) was incubated with increasing peptide concentrations (0, 2, 5, 10, 15, 20, 40, 80, 160 and 200 μM). The intensity of free tandem (I_P), tandem with 1 and 2 peptides (I_{PL} and I_{PL2}) was recorded for charge states referring to native protein or complex (i.e. 9+, 10+, 11+ and 12+).

To determine binding stoichiometry, the full-length human HSP90 (HSP90βFL) concentrated at 10 μM was incubated with increasing TPR tandem concentration (0, 5, 10, 20 and 40 μM), and analyzed on Synapt G2 HDMS with the following parameters: Vc 180 V, Pi 6 mbar.

For Pih1D1:RPAP3 complexes analysis, an aliquot was directly analyzed by non-denaturing MS (D0 sample) while another one was further incubated at 20°C for 7 days (D7 sample). Samples were then diluted to 5 μM in 300 mM ammonium acetate pH6.9 buffer for non-denaturing MS injection. Non-denaturing MS analyses were carried out on an ESI-TOF mass spectrometer (LCT from Micromass Waters upgraded for high mass by MS Vision) coupled to an automated chip-based nanoelectrospray system (Triversa Nanomate, Advion, Ithaca, U.S.A.) operating in the positive ion mode. Calibration was performed using singly charged ions produced by a 2-g/L solution of cesium iodide (Acros organics, Thermo Fisher Scientific, Waltham, MA, USA) diluted in 2-propanol/water (50/50 v/v). Instrumental parameters were optimized for the detection of fragile noncovalent complexes by increasing the interface pressure to 6 mbar and the cone voltage to 100 V. Data interpretation was realized with MassLynx 4.1 software (Waters, Manchester, UK).

IP-LUMIER Assays

HEK-293T cells were transfected with FFL-RPAP3 and RL-HSP90 plasmids and grown at 37°C, 5% CO_2 in Dulbecco's modified Eagle medium (DMEM, Sigma Aldrich, France) added by 10% FBS, 2.9 mg/mL glutamine and 10 U/mL penicillin/streptomycin. For LUMIER assays, 24-well plate cells were extracted with 500μl of HNTG (20 mM HEPES, pH 7.9, 150 mM NaCl, 1% Triton, 10% glycerol, 1 mM $MgCl_2$, 1 mM EGTA, and protease inhibitors (Roche)), 48 hours after transfection. For immunoprecipitation, 96-well plate was coated overnight with anti-Flag antibody (M2, Sigma), incubated 1 hour with blocking buffer (PBS with 3% BSA, 5% sucrose and 0.5 % Tween 20). Control IP is done with wells not incubated with antibody. For each extract, IP well and control IP well are filled with 100μl and incubated for 3 hours at 4°C. Wells were washed five times in HNTG before luciferase reading using Dual Luciferase kit (Promega). To read input, 2μl of each input is added in separated wells. Finally, for each extract, we measure FireFly and Renilla luciferase activity in three wells (input, IP and control IP without antibody). Firefly (FFL) and Renilla (RL) signals of IP and control IP are normalized with input:

$$\%coIP = 100 * \frac{RL(IP)/50 * RL(Input)}{FFL(IP)/50 * FFL(Input)}$$

To compare IP specificity (Fold), %coIP of IP is next compared to %coIP of control IP:

$$Fold = 100 * \frac{RL(IP)/RL(Input)}{RL\ (Contrôle)/RL(Input)}$$

Plasmids Used for Studying the HSP90 Chaperone Cycle

Homo sapiens RPAP3 isoform 2 coding sequence was cloned in fusion with an amino-terminal hexahistidine (N-His_6) tag in a plasmid derived from pET21a. Truncation 133-396 was subcloned with an N-His_6 in pCDFDuet site 1. Sequence coding for full-length Saccharomyces cerevisiae Hsp82 was cloned in a pRSFDuet in fusion with an amino-terminal His_6-Smt3 sequence. Mutants used for Cy-fluorophore labelling were generated by site directed mutagenesis with a variation of the quick-change protocol from wild-type sequence cloned in pRSETa. Sequence coding for Homo sapiens $Hsp90\alpha_{FL}$, $Hsp90\alpha_{MC}$ and $Hsp90\beta_{FL}$ were cloned in plasmids pET28a (Hsp90α) and pRSETa ($Hsp90\beta_{FL}$) dowstream of N-Hi_6. Accurate insertions of UNIPROT reference sequences, in phase with reading frame, were validated by sequencing (MWG Eurofins Genomics).

Expression Strains Used for Studying the HSP90 Chaperone Cycle

Plasmids were used to transform chemicompetent *E. coli* BL21(DE3) Rosetta2-pLysSRAR strain (Millipore), transformants grown on LB medium containing 50 μg/mL kanamycin, 150 μg/mL ampicillin, 50 μg/mL streptomycin, or 34 μg/mL chloramphenicol, for relevant plasmid of interest resistance. Saturated precultures were stored in 20% (v/v) glycerol at -20°C and used to initiate subsequent overexpressions.

Overexpression at 30°C for 3 h was induced by addition of 0.5 mM IPTG in 2xYT medium supplemented with antibiotics at OD(680nm)=0.8. Hsp90α/β expression strains were grown at 30°C, and induced at 18°C overnight. Cell pellets were collected by 4,000 rcf centrifugation for 15min.

Proteins Used for Studying the HSP90 Chaperone Cycle

Cell pellets were resuspended in 50 mL lysis buffer HisA (25 mM Tris-Cl pH=8.0; 500 mM NaCl; 20 mM Imidazole pH=8.0), cells wall and membrane were disrupted by 2 cycles of CellD at 1,36 kbar. Crude lysates were clarified by 30,000 rcf centrifugation for 30 min and loaded on Ni-affinity resin on Äkta FPLC at 0.5 mL/min. 50 CV washed bound proteins were eluted over a 10 CV linear gradient of 20 mM to 300 mM Imidazole and collected fractions containing proteins were pooled and concentrated to 10 mL by ultrafiltration (Millipore). Proteins were further subjected to size-exclusion chromatography through Superdex200 16/60 (GE Healthcare), and eluted over an isocratic gradient of buffer GF (50 mM Tris-Cl pH=8.0; 150 mM NaCl; 0.5 mM EDTA pH=8.0). Peaks containing proteins of interest, as assessed by SDS-PAGE, were pooled and concentrated to 20 mg/mL before being snap-frozen and stored at -80°C. His_6-Smt3-fused proteins were cleaved for 30 min at room temperature by His_6-$Ulp1_N$-His_6 at an enzyme:substrate mass ratio of 1:35. His_6-Smt3 and His_6-$Ulp1_N$-His_6 were retained on 4 mL Ni-NTA resin (Sigma-Aldrich). Hsp90α/β were further purified on Tosoh-Q G650 anion exchange resin, eluted over a linear gradient of 50 mM to 1000 mM NaCl. Hsp90α/β final clearance of ATPase contaminants was performed with a spatula tip of ATP-agarose resin, retained on a 0.20 μm filter.

Analytical Size-Exclusion Chromatography

Specific elution volumes of pure proteins or complex mixes were determined on size-exclusion chromatography through a Superose6 10/300 Increase column (GE Healthcare). ~1 nmol sample was applied in a 100 μL dilution. Isocratic elution at 0,4 mL/min was done in buffer GF. Apparent molecular weights were calculated according to a calibration mix of globular standards (Bio-Rad #1511901).

Kinetic ATPase Assay

Steady-state ATPase activity of Hsp90 was reported by PK-LDH catalyzed oxidation of NADH as described earlier (Eckert et al., 2010; Panaretou et al., 1999) in 100 μL on 96 well plates or in 55 μL in cuvettes. The reaction buffer was changed to 50 mM Hepes/KCl, 150mM NaCl, 2mM ATP pH=8.5 mM $MgCl_2$. Background, Hsp90-independent, ATPase activity was determined by the addition of 30 μM geldanamycin and systematically substracted. Measures were performed in 5 replicates.

Dimer Subunits Exchange

Hsp90 dimer half-life was measured by Förster fluorescence energy transfer (Retzlaff et al., 2010) between maleimide derived Sc-Hsp90mQ385C-Cy3 at 0,5 μM and Sc-Hsp90mQ385C-Cy5 at 0,5 μM with $\lambda_{excitation}$=350 nm and $\lambda_{emission}$=580 nm on a Cary eclipse fluorimeter. Kinetic FRET decrease after addition of 20 μM unlabelled Sc-Hsp90 was measured for 600 sec; FRET dimer half-life was computed as ln2/b, in y = y0 + a*exp(b/x) as the exponential decay of dimeric species. Effect of cochaperones at 160 μM was assayed in the same conditions.

Cell Culture and RT-PCR

A549 lung adenocarcinoma and Kato-III gastric carcinoma cells were purchased from European collection of cell cultures, UK; primary culture of dermal fibroblasts (AG08470) from a healthy female were purchased from Coriel Cell Repositories (Camden, NJ); primary culture of dermal healthy fibroblasts (2015-03784, ICL) from female patient treated with radiotherapy for breast cancer were obtained from Institut de Cancerologie de Lorraine (ICL, Vandoeuvre-les-Nancy, France) and HeLa S3 and HEK-293 cells were obtained from the Institut de Génétique et de Biologie Moléculaire et Cellulaire (IGBMC, Strasbourg, France). A549, HeLa S3, HEK-293 and dermal fibroblast cells were cultured in Dulbecco's modified Eagle medium (DMEM, Sigma Aldrich, France) and Kato-III in RPMI medium 1640 (Gibco by Invitrogen, France). All media were supplemented with 2 mM L-glutamine, penicillin/streptomycin and 10% fetal calf serum (Dutscher, France) for A549, HeLa S3, HEK-293, 15% for dermal fibroblasts and 20% for Kato-III cells.

For stress analysis, exponentially growing cells were plated twenty-four hours before stress induction. Mild heat shock was performed by submersion of cells in a temperature-regulated circulating water bath at 42°C for 1h or 2h, followed by recovery at 37°C for 1h. For oxidative stress, cells were exposed to 500μM H_2O_2 (Sigma Aldrich, France) for various periods of time (24h or 4h). Ionizing radiations were performed on a 6-MeV γ-ray clinical irradiator (iX VARIAN) at the Institut de Cancerologie de Lorraine (ICL, Vandoeuvre-les-Nancy, France) at a dose of 2 or 10 Gy, with a dose rate of 6 Gy min^{-1}.

Total RNAs were extracted from cells with TRIzol (Invitrogen). RNAs (0.5μg) were treated with RQ1 DNase (Promega, Charbonnieres, France) and reverse transcribed using random hexamer and dT oligonucleotides mix and MMLV retrotranscriptase (Promega) according to the manufacturer's instructions. PCR was carried out with 200 nM dNTP mix and 25U DreamTaq DNA pol (Fisher Scientific, Illkirch, France). Denaturation, annealing, and extension steps were performed for 30 sec at 94°C, 58°C, and 72°C respectively, for 35 cycles. The splicing products were fractionated on 2% agarose gel.

SILAC-IP and Proteomic Analysis

HeLa cells were grown for 15 days in each isotopically labeled media (CIL/Eurisotop), to ensure complete incorporation of isotopically labeled arginine and lysine (light label [K0R0, L] or heavy label L-Lysine-^{2}HCl [^{2}H4, 96–98%]/L-Arginine-HCl [^{13}C6, 99%] [K4R6, M]; percentages represent the isotopic purity of the labeled amino acids). Eight 15-cm diameter plates were used per SILAC condition. Cells were rinsed with PBS, trypsinized and cryogrinded in lysis buffer (20 mM HEPES, pH 7.4, 150 mM NaCl, 0.5% triton X-100, protease inhibitor cocktail). Extracts were incubated 20 min at 4°C and clarified by centrifugation for 10 min at 20,000 g. For all IP experiments, extracts were pre-cleared by incubation with Protein G Sepharose beads (GE healthcare) for 1 h at 4°C. The control

was extracted from the SILAC light condition prepared from H9 HeLa cells that did not express the GFP fusion. Each extract was then incubated with 50 µl of GFP-Trap beads (gta-20, Chromotek) for 75 min at 4°C, washed five times with lysis buffer, and beads from the different isotopic conditions were finally pooled. Bound proteins were eluted by adding 1% SDS to the beads and boiling for 10 min. Reduction and alkylation were performed on the eluate with DTT (BDH 443553B, 10 mM) for 2 min at 95°C followed by iodoacetamide treatment (Sigma I1149, 50 mM) for 30 min in the dark. Proteins were separated by SDS/PAGE and in gel-digested with trypsin in 20mM NH_4HCO_3 (Trypsin Gold, Promega V5280). Ten slices were cut, and extracted peptides were resuspended in 0.1% formic acid/2% acetonitrile solution before being analyzed by mass spectrometry. Peptides were analyzed by nano-flow liquid chromatography coupled to Fourier transform tandem mass spectrometry (nanoLC-FT-MS/MS) using a LTQ Velos Pro Orbitrap Elite mass spectrometer coupled to an Ultimate 3000 (Thermo Fisher Scientific). Desalting and pre-concentration of samples were performed on-line on a Pepmap precolumn (0.3 mm 10 mm, Thermo Fisher Scientific) in buffer A (2% acetonitrile, 0.1% formic acid). A gradient consisting of 2–40% buffer B (B = 99.9% acetonitrile with 0.1% formic acid; 3–33 min) and 40–80% B (33–34 min) was used to separate peptides at 300 nL/min from a Pepmap capillary reversed-phase column (0.075mm× 150 mm, Thermo Fisher Scientific). Mass spectra were acquired using a top-20 collision-induced dissociation (CID) data-dependent acquisition (DDA) method. The Orbitrap was programmed to perform a FT 400–1,400 Th mass scan (60,000 resolution) with the top 20 ions in intensity selected for collision-induced dissociation (CID) datadependent acquisition (DDA) MS/MS in the LTQ. FT spectra were internally calibrated using a single lock mass (445.1200 Th). Target ion numbers were 500,000 for FT full scan on the Orbitrap and 10,000 MSn on the LTQ. Data were acquired using the Xcalibur software v2.2. Protein identification and quantitation were performed using the program MaxQuant (version 1.5.2.8; http://www.maxquant.org/). Few parameters were not default: database: human reference proteome set (canonical isoforms downloaded from Expasy on May 29th 2017); enzyme specificity trypsin/P; variable modifications: methionine oxidation and protein N-Acetylation; Fixed modifications: Cysteine carbamidomethylation; MS/MS tolerance: 0.5 Da; False Discovery Rate (FDR): 1%. In addition to the FDR, proteins were considered to be identified if they had at least two peptides including one unique/Razor peptide and they were considered quantified if they had at least one quantified SILAC pairs. Proteins labeled as REV (non-real proteins from the reverse database) and CONT (contaminants) were automatically discarded, as well as proteins that did not show any SILAC M/L, H/L and H/M ratio. B Significance calculations were done with the software Perseus v1.4.2 to highlight statistically significant protein ratios (p value < 0.05).

Protein Coexpression Assays

DNA sequence of several fragments of PIH1D1 and RPAP3 were cloned respectively into pnEA (for his-tagged protein) and pnYK (for native protein) vectors. Co-expression was performed in *E. coli* BL21(DE3) pRARE2 bacteria. Ca2+-competent cells were co-transformed with pnEA and pnYK vectors using a heat-choc at 42°C and spread on a solid LB-medium supplemented with ampicillin, chloramphenicol and kanamycin. After one night at 37°C, a clone was grown at 37°C in liquid LB medium until DO_{600} reached ~ 0.6. Protein expression was induced by 0.3 mM IPTG and bacteria were placed at 20°C under agitation overnight. Cells were harvested and sonicated in 25mM HEPES, pH 7.5, NaCl 300 mM, 10 mM Imidazole, 0.5 mM TCEP. Supernatant was incubated on TALON beads for 2 hours. Proteins were eluted from the beads using loading buffer. The purification was followed on 12.5% SDS-Polyacrylamide gels.

Purification of the $RPAP3_{281-445}$:$PIH1D1_{199-290}$ Complex

The DNA sequence corresponding to region 199-290 in PIH1D1 were cloned into a pnEA-3CH plasmid (for his-tagged protein) and the DNA sequence corresponding to region 281-445 in RPAP3 was cloned into a pnYK plasmid (for native protein) vectors. Ca2+-competent BL21(DE3) pRARE2 *E. coli* bacteria were co-transformed using a heat-choc at 42°C and spread on a solid LB-medium supplemented with ampicillin, chloramphenicol and kanamycin. After one night at 37°C, a clone was grown at 37°C in liquid LB medium until DO_{600} reached ~ 0.6. Protein expression was induced by 0.3 mM IPTG and bacteria were placed at 20°C under agitation overnight. Cells were harvested and sonicated in 25mM HEPES (pH 7.5), 300 mM NaCl, 10 mM Imidazole, 0.5 mM TCEP. Supernatant was incubated on TALON beads. Elution from the beads was performed using the 3C-prescission protease. A final size-exclusion chromatography in 10 mM NaPi (pH 6.4), 150 mM NaCl, 0.5 mM TCEP (NMR buffer) permitted to recover pure protein fractions. The purification was followed on denaturing 12.5% SDS-Polyacrylamide gels. Fractions corresponding to the desired protein complex were pooled and concentration was assessed using molar extinction coefficient at 280 nm.

Crystallization, Data Collection and Structure Determination of the $RPAP3_{281-445}$:$PIH1D1_{199-290}$ Complex

100 nL drops of protein complex were mixed with 100 nL of mother liquor of the PEGsII sparse-matrix screen, and let to equilibrate by vapor diffusion against a reservoir of 50 µL mother liquor. Plate-shaped, diffracting crystals of ~50 µm in the largest dimension grew in 7 days at 20°C in 100 mmol.L^{-1} $CaCl_2$, 30 % (w/v) PEG-3350, 100 mmol.L^{-1} Tris-Cl pH=7.5. Optimized crystals were obtained on a bidimensional gradient of $CaCl_2$ and PEG-3350, at final respective concentrations of 50 mmol.L^{-1} and 25%.

Crystals were vitrified after equilibration in mother liquor supplemented with 25% (v/v) ethylene glycol. X-rays diffraction at ESRF beamline ID30-A Massif-2 yielded a complete dataset at a resolution of 2.97 Å, reduced and scaled by XDS (Table 1).

Crystallographic data analysis, phasing and molecular modelisation were performed in the PHENIX suite of crystallographic softwares using RPAP3-TPR2 NMR structure (this study) and $PIH1D1_C$ ROBETTA predicted structure as search models (Adams et al., 2010). 2 RPAP3 and 2 PIH1D1 were present in the asymmetric unit, according to Matthews analysis of the crystal density. Continuous electron density in the resulting maps was used to automatically build the polypeptides. Cycles of manual building in

COOT (Emsley and Cowtan, 2004) and refinement with PHENIX.REFINE (Afonine et al., 2012) were applied until maximal occupancy of the density and satisfactory R/R-free were reached.

QUANTIFICATION AND STASTISTICAL ANALYSIS

For all experiments, details on the quantification and statistical methods are given in the concerned paragraphs of the Method Details section.

DATA AND SOFTWARE AVAILABILITY

NMR structures and chemical shifts of $RPAP3_{133-255}$, $RPAP3_{281-396}$:DTSRMEEVD, $RPAP3_{281-396}$:SGPTIEEVD and X-ray structure of $RPAP3_{281-445}$:$PIH1D1_{199-290}$ were deposited in the Protein Data Bank under accession numbers 6FD7, 6FDP, 6FDT and 6GXZ respectively.